Separation and Purification Technology 371 (2025) 133360

Contents lists available at ScienceDirect

Separation and Purification Technology

journal homepage: www.elsevier.com/locate/seppur

Tailoring MXene composition and structure for High-Performance mixed matrix membranes in CO_2 separation applications

Abtin Ebadi Amooghin [a,*], Ahmad Arabi Shamsabadi [b,*], Mohammad Mehdi Moftakhari Sharifzadeh [c], Amirali Salehi [d], Hamidreza Sanaeepur [a], Mostafa Dadashi Firouzjaei [e], Vahid Rad [f], Hesam Jafarian [e], Mark A. Elliott [e], Hermenegildo Garcia [g,*]

[a] Department of Chemical Engineering, Faculty of Engineering, Arak University, Arak 38156-8-8349, Iran
[b] Department of Chemistry, University of Pennsylvania, Philadelphia, PA 19104, USA
[c] Department of Chemical Engineering, Science and Research Branch, Islamic Azad University, Tehran, Iran
[d] Faculty of Chemical Engineering, Tarbiat Modares University, Tehran, Iran
[e] Department of Civil, Environmental and Construction Engineering, University of Alabama, Tuscaloosa, AL 35487, USA
[f] Department of Chemical Engineering, Drexel University, Philadelphia, PA 19104, USA
[g] Departamento de Química/Instituto Universitario de Tecnología Química CSIC-UPV, Universitat Politècnica de València 46022 Valencia, Spain

ARTICLE INFO

Editor:Gaohong He

Keywords:
Mixed Matrix Membranes
Mo_2TiC_2
Ti_2C
V_2C
and CO_2/N_2 separation

ABSTRACT

Incorporating two-dimensional (2D) nanomaterials into polymer matrices can be an effective strategy to increase the performance of membranes, overcoming the permeability/selectivity trade-off. So far, MXene-based gas separation mixed matrix membranes (MMMs) have been limited to Ti_3C_2 and they demonstrated high gas separation performance. However, information about the influence of composition and structure of MXene on the performance of MMM is still lacking. Herein, a systematic investigation of the effect of the chemical composition and number of layers of MXenes on the CO_2 transport properties of MMMs is reported. Mo_2TiC_2, Ti_2C and V_2C MXenes were incorporated into a Pebax-1657 matrix. The results revealed that the number of MXene layers considerably affects the dispersion of MXenes in the polymer matrix that contain crystalline and amorphous domains, M_3C_2 MXenes (Mo_2TiC_2 and Ti_3C_2) improve membrane separation more than M_2C MXenes (Ti_2C and V_2C). In addition, in the case of M_3C_2 MXenes (Mo_2TiC_2 and Ti_3C_2), composition strongly affect the dispersion of nanosheets in the polymer, as confirmed by X-ray diffraction and mechanical properties analysis. Molecular dynamics (MD) simulation combined with gas permeation models further confirmed the excellent compatibility of MXenes with the polymer chains. Significant improvement in CO_2 permeability (up to 70%) and CO_2/N_2 separation selectivity (up to 137%) was achieved, placing MXene MMMs above the 2008 Robeson upper bound, implying defect-free interfaces and excellent matrix dispersion. Finally, the impact of feed composition, temperature, and pressure on gas separation performance of the MMMs was fully investigated. Our findings indicate the tremendous potential that tuning MXene properties can have for the development of high-performance gas separation membranes.

1. Introduction

Highly selective membranes are required to recover target species and remove pollutants in gas separation processes.[1–7] The development of mixed matrix membranes (MMMs), a class of composite membranes composed of polymers/fillers, is an effective approach to surpass the so-called upper bounds of traditional polymeric membranes.[8,9] The addition of fillers with nanoscale dimensions can not only increase the free volume of matrices for faster diffusion, but also impose further entropic force for selective recognition of gas species, thereby leading to significant improvement of transport properties.[10,11] The development of MMMs containing new fillers with improved permeability and selectivity is key to the technological revolution.[12,13] Excellent interfacial compatibility of the filler-matrix is a prerequisite for realizing

* Corresponding authors.
E-mail addresses: a-ebadi@araku.ac.ir (A. Ebadi Amooghin), neginali@sas.upenn.edu (A. Arabi Shamsabadi), hgarcia@qim.upv.es (H. Garcia).

https://doi.org/10.1016/j.seppur.2025.133360
Received 21 January 2025; Received in revised form 26 April 2025; Accepted 1 May 2025
Available online 5 May 2025
1383-5866/© 2025 Elsevier B.V. All rights are reserved, including those for text and data mining, AI training, and similar technologies.

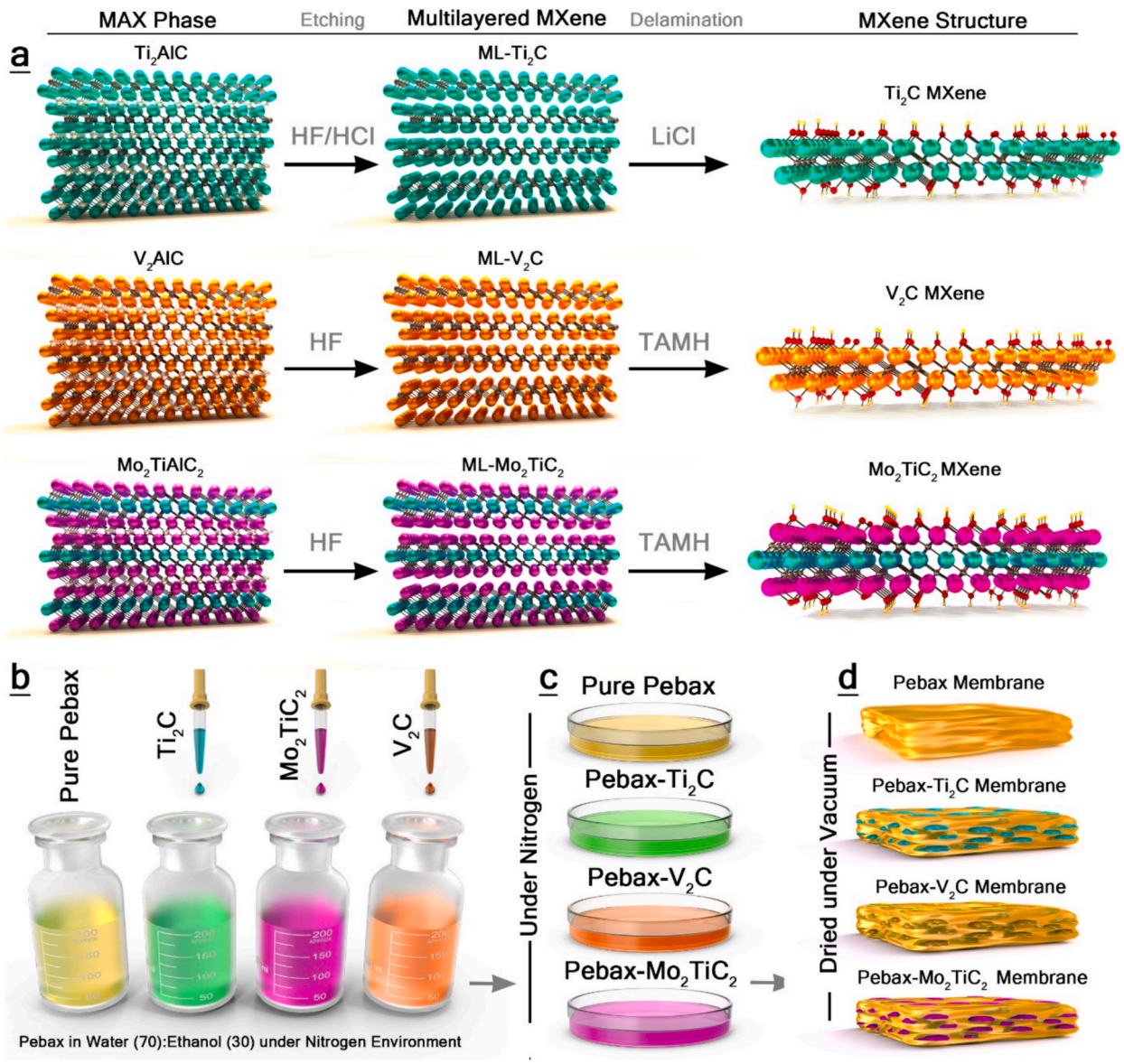

Fig. 1. Schematic representation of (a) synthesis and delamination of Mo_2TiC_2, Ti_2C, and V_2C MXenes, and (b) the fabrication steps of the free-standing MMMs.

the high separation potential of these hybrid membranes.[9] Two-dimensional (2D) nanomaterials bearing functional groups are ideal fillers for fabricating defect-free MMMs, even in ultra-thin formats, due to their high interfacial area and strong interfacial interactions.[14].

MXenes are a large expanding family of 2D transition metal carbides and nitrides finding abundant applications in separation processes.[14–17] MXenes have the general formula of $M_{n+1}X_nT_X$, where M is an early transition metal, X denotes carbon and/or nitrogen, n = 1–4, and T corresponds to the surface functionalities (–OH, =O, and −F).[18] MXenes have attracted considerable attention due to tunable interlayer galleries, high aspect ratio, rich surface chemistry, and versatile chemical composition and number of layers in the structure. In the only precedent in MXene-based MMMs Ti_3C_2 MXene was used in combination with Pebax, observing a fast and selective CO_2 transport.[19] It was found that the polymer chains protect Ti_3C_2 MXene nanosheets against oxidation, Pebax-1657/Ti_3C_2 membranes demonstrating stable gas separation performance after storage in the ambient conditions for six months.[19].

Since all MXene-based MMMs for gas separation studied so far have been prepared using Ti_3C_2, information about the influence of composition and structure of MXene on the performance of MMM is still lacking. [19] It is, therefore, necessary to determine which can be the optimal MXene composition and number of layers to achieve an enhanced transport properties and selectivity of polymer membranes. Theoretical calculations predicted that transition-metal composition, atomistic structure, and surface chemistry should change the properties of MXenes, but experimental data supporting these claims are missing. Studying the effect of the surface chemistry of MXenes is very challenging due to the coexistence of different surface functionalities, relatively strong M−T bonds, and the metastable nature of MXenes. To fabricate advanced MXene-based membranes, it is necessary to determine the relationship between composition/atomistic structure and gas transport properties and to generate a dataset of MXene membranes with diverse permeability and selectivity.

Herein, we report a systematic investigation on the role of MXenes to improve the gas transport properties of Pebax-1657 membranes, a widely-used polyether block amide membrane [20,21] for CO_2 separation. The choice of Pebax-1657 matrix is based on rich functional groups in the backbone generating crystalline and amorphous domains and providing excellent interfacial compatibility. Pebax-1657 matrix also allows a straightforward comparison of our MMMs with the reported Pebax-1657-Ti_3C_2 MXene-based ones for gas separation.[22–24] While

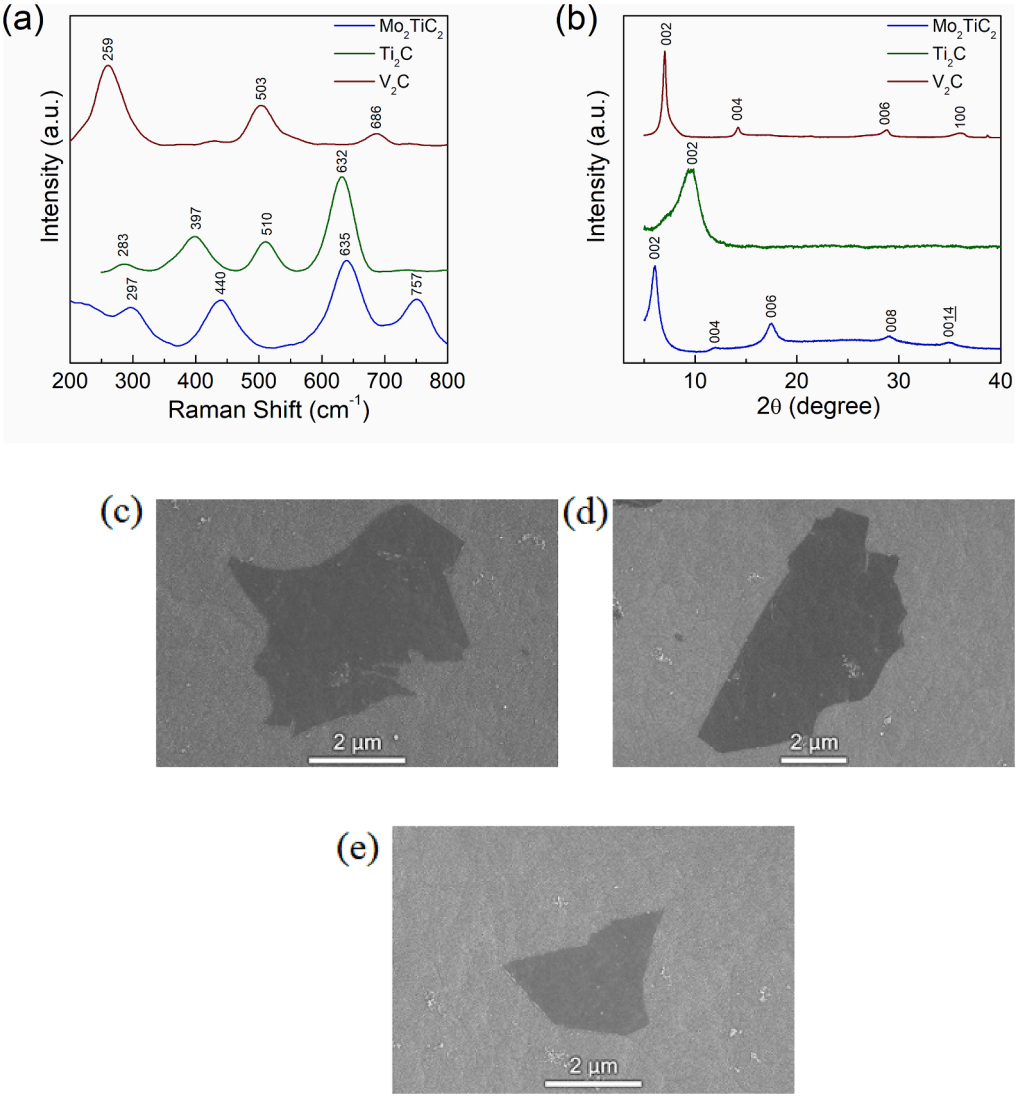

Fig. 2. (a) Raman spectra of Mo_2TiC_2, Ti_2C, and V_2C MXenes, (b) XRD patterns of Mo_2TiC_2, Ti_2C, and V_2C MXenes, SEM images of (c) Mo_2TiC_2, and (d) Ti_2C, and (e) V_2C.

prior studies have exclusively focused on Ti_3C_2 MXene in Pebax membranes, our work is the first to systematically explore how different MXene compositions- Mo_2TiC_2, Ti_2C, and V_2C- impact membrane performance. By investigating their atomistic structures and chemical compositions, we provide crucial experimental validation for theoretical predictions on MXene surface chemistry and transport properties, which were previously unexplored. Furthermore, we explicitly define the state-of-the-art in MXene-based gas separation membranes, detailing the challenges of achieving optimal permeability and selectivity through filler-polymer compatibility. Our study introduces a new dataset of MXene-based membranes, shedding light on the correlation between MXene structure and gas transport properties. By incorporating molecular dynamics (MD) simulations, we also provide mechanistic insights into MXene-polymer interactions.

2. Experimental

2.1. Materials

Mo_2TiAlC_2, Ti_2AlC, and V_2AlC MAX powders were supplied from American Elements. Hydrofluoric acid (HF, ACS reagent, 48 %), hydrochloric acid (HCl, ACS reagent, 37 %), lithium chloride (LiCl, ACS reagent, ≥99 %), and tetramethylammonium hydroxide (TMAH, 25 wt % in H_2O) were purchased from Millipore-Sigma and used without further purification. Pebax-1657 was obtained from Arkema Inc., France. Carbon dioxide and nitrogen gases (>99.99 %) were purchased from Saman Gas Co., Arak, Iran.

2.2. Synthesis of MXenes

Ti_2C was produced via etching of Ti_2AlC MAX with a solution containing HF and HCl. First, 6 mL of deionized (DI) water and 12 mL of HCl were mixed with 2 mL of HF. Next, 1 g of the MAX powder was added slowly to the solution at room temperature under stirring. The temperature was increased to 35 °C and the mixture was stirred for 24 h at 300 rpm. After the reaction completion, DI water was added to the mixture followed by centrifuging at 3500 rpm for 2 min and this washing process was repeated several times until the pH value is > 6. The sediment was added to 50 mL of a 20 mg/mL LiCl solution. The temperature was increased to 35 °C and the mixture was stirred for 8 h at 300 rpm. Then, the suspension was centrifuged at 3500 rpm for 10 min. Centrifugation was repeated until obtaining black supernatant suspensions. The supernatant containing large Ti_2C flakes was collected and centrifuged at 7500 rpm for 3 min and used for fabrication of Ti_2C films.

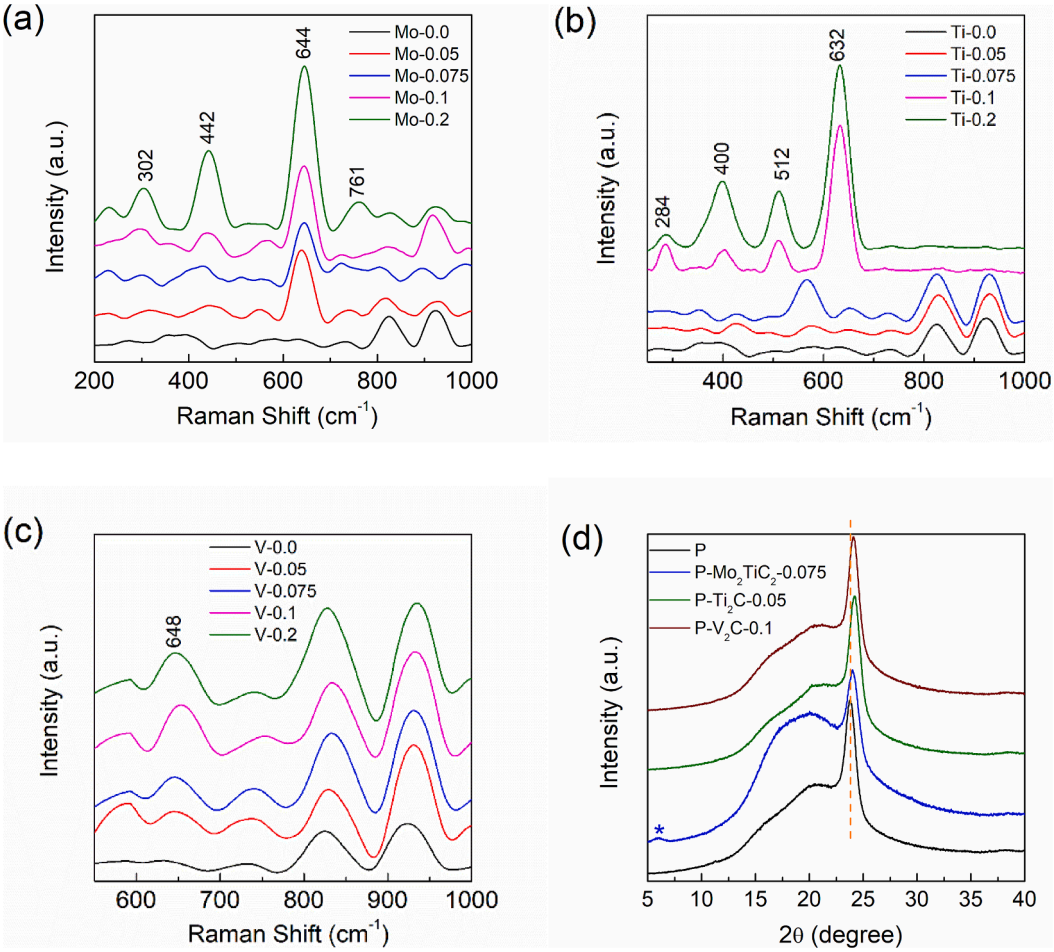

Fig. 3. (a) Raman spectra of Pebax-Mo_2TiC_2 membranes, (b) Raman spectra of Pebax-Ti_2C membranes, (c) Raman spectra of Pebax-V_2C membranes, (d) XRD patterns of Pebax-Mo_2TiC_2-0.075 wt%, Pebax-Ti_2C-0.05 wt%, and Pebax-V_2C-0.1 wt% MMMs, (e) elastic modulus of Pebax-Mo_2TiC_2, Pebax-Ti_2C, and Pebax-V_2C membranes at different MXene loadings, (f) elongation at break of Pebax-Mo_2TiC_2, Pebax-Ti_2C, and Pebax-V_2C membranes at different MXene loadings, and (g) tensile strength of Pebax-Mo_2TiC_2, Pebax-Ti_2C, and Pebax-V_2C free standing membranes.

Mo_2TiC_2 and V_2C were produced via etching of Mo_2TiAlC_2 and V_2AlC MAX phases, respectively. First, 1 g of each MAX powder was added slowly to a 20 mL HF solution at room temperature under stirring. The temperature was increased to 50 °C for Mo_2TiC_2 and 35 °C for V_2C and the mixture was stirred for 48 h at 300 rpm. After the reaction completion, DI water was added to the mixture followed by centrifuging at 3500 rpm for 2 min and this washing process was repeated several times until the pH value is > 6. The sediment was added to 20 mL of a 50 mg/mL TMAH solution and the mixture was stirred for 12 h at room temperature. The mixture was then centrifuged several times with DI water at 9000 rpm for 10 min, until obtaining a pH value below 8. Finally, the suspension was centrifuged at 3500 rpm for 10 min. Centrifugation was repeated until obtaining black supernatant suspensions. The supernatants containing large Mo_2TiC_2 or V_2C flakes were collected and centrifuged at 7500 rpm for 3 min and used for fabrication of films.

2.3. Membrane fabrication

3 % homogenous Pebax-1657 solution was prepared by dissolving polymer beads in water/ethanol (70/30 wt%). The solution was poured into a Teflon coated petri dish and after solvent evaporation at room temperature the pristine membrane was obtained. Mixed matrix membranes (MMMs) with various concentrations of MXenes (0.05, 0.075, 0.1, and 0.2 wt%) were fabricated from Pebax-MXene solutions prepared by adding different MXenes colloidal solutions (Mo_2TiC_2, Ti_2C, and V_2C) to the 3 % Pebax solutions. The polymer-MXene mixtures were poured into Teflon coated petri dishes and were kept under N_2 to obtain films after solvent evaporation at room temperature. All the membranes were dried under vacuum at 80 °C for 18 h. a schematic representation of the synthesis of MXenes, and MMMs is shown in Fig. 1.

3. Results and Discussion

We produced Ti_2C by etching its corresponding MAX phase using a mixture of HF and HCl followed by delamination using LiCl. Instead, Mo_2TiC_2 and V_2C were synthesized through HF etching of their parent MAX phases and then were delaminated by intercalation of tetramethylammonium hydroxide (TMAH) (Fig. 1). To confirm the structures of the synthesized MXenes, Raman spectroscopy (Fig. 2**a**) and X-ray diffraction (XRD) (Fig. 2**b**) were conducted on MXene films fabricated from their aqueous colloidal solutions using vacuum-assisted filtration. The broadening and shifting of Raman bands (Fig. 2**a and** Fig. S2**a-c**), along with the emergence of peaks associated with surface functional groups, confirm the successful removal of the Al layers and the formation of multilayer MXene structures. The band at 440 cm^{-1} in the Raman spectrum of Mo_2TiC_2 can be ascribed to the oxygen dominated vibrational mode along the basal plane.[25,26] The higher bands at 635 and 757 cm^{-1} can be related to carbon atoms parallel (E_g) and perpendicular (A_g) to the basal plane, respectively. In the Raman spectrum of Ti_2C, the

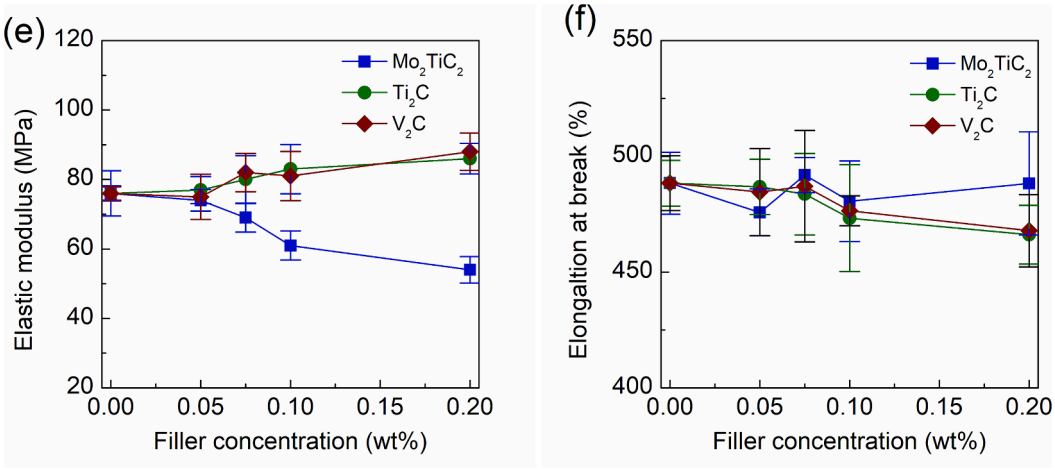

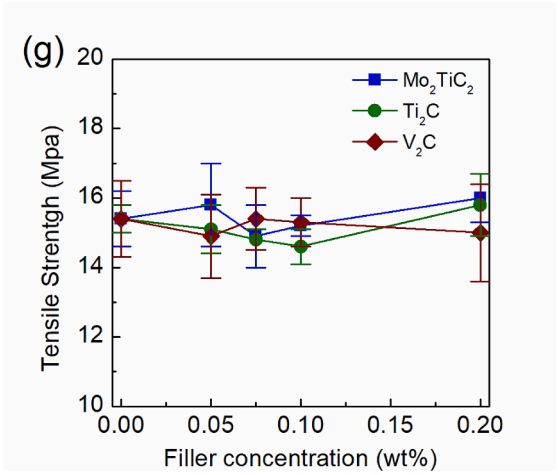

Fig. 3. (*continued*).

out-of-plane stretching vibrations of Ti and C along with the termination of =O, −F, and –OH appear at 283 cm^{-1} (mostly −F group).[27,28] The vibrational bands at 397, 510, and 632 cm^{-1} are generated from the Ti-C non-stoichiometric and C–C bonds.[29] In the Raman spectrum of V_2C, three main frequency modes were observed at 259, 503, and 686 cm^{-1}. The first band is corresponding to the in-plane vibrations of V atoms. The second Raman frequency appeared around 503 cm^{-1} due to the surface termination with −F and –OH groups.[30,31] The higher frequency modes are obviously indicative of surface terminated V_2C. Although the theoretical approaches could not explain the Raman band at 686 cm^{-1}, this band can be attributed to the heterogeneous and randomly distributed functional groups. Our Raman spectra agree well with numerous experimental and simulation studies. [27–31] The disappearance of characteristic MAX phase peaks (**Fig. S3a-c**) and the emergence of the (002) peak at lower angles in XRD of MXenes (Fig. 2**b**) confirm successful Al-layer removal and formation of multilayer MXene structures. The position of the (002) peak is 6.02, 9.64, and 6.98 Å for Mo_2TiC_2, Ti_2C, and V_2C, respectively. In addition to Raman spectroscopy, the good agreement of XRD patterns with previous studies further confirms the successful synthesis of Mo_2TiC_2, Ti_2C, and V_2C MXenes.[25,32–34] Scanning electron microscopy (SEM) images (Fig. 2**c-e**) show the morphology and size of individual MXene flakes. For each MXene (V_2C, Ti_2C, and Mo_2TiC_2) the images highlight the characteristic 2D structure of the flakes. The observed single flakes have lateral dimensions ranging from approximately 2 to 6 μm, depending on MXene type.

Dispersion of all three MXenes up to 0.2 wt% concentration could not be detected in the hybrid matrices via Fourier transform infrared spectroscopy (FTIR) (Supporting Information, **Fig. S4a-c**). Compared to the pristine Pebax, similar bands with no shifts were observed in the FTIR spectra of the hybrid membranes. Despite strong hydrogen bonds between MXene surfaces and polymer chains, MXenes are not detectable in FTIR spectra because of their low concentrations and surrounding the nanosheets with the polymer chains as also was observed for embedded Ti_3C_2 and MoS_2 in Pebax.[35] The dispersion of all three MXenes above 0.05 % concentrations in the Pebax matrix can be verified in the Raman spectra of all MMMs (Fig. 3**a-c**) compared to the spectrum of the pristine polymer. For MMMs containing different MXenes, the extra peaks observed in the spectra originate from MXenes which are in perfect agreement with the previously discussed Raman frequencies of MXenes (Fig. 2**a**). Distinctive changes in terms of the Raman shift in the peaks above 600 cm^{-1} were observed for MMMs containing Mo_2TiC_2 and V_2C. The peak shift indicates the interactions between the Pebax chains and the heterogeneous surface termination groups of the MXenes. In addition, Raman spectroscopy analysis indicated that mixing MXenes with Pebax does not induce structural defects in the polymer matrix.

The tendency of MXenes with diverse atomistic structures and compositions toward the amorphous (polyethylene oxide, PEO) or crystalline (polyamide, PA) domains of Pebax can be qualitatively obtained by XRD analysis. Two distinct diffraction peaks in all MMMs including a broad peak at 2θ ~ 15-20° and a narrow peak at around 2θ ~ 24° reflect the soft (PEO) and hard (PA) segments of the polymer, respectively, in all hybrid membranes (**Fig. S5a-c**, SI). No significant change was observed in the spectra of V_2C- and T_2C-based MMMs was observed, except for a slight shift toward higher angles with increasing filler content. This shift suggests the effective dispersion of Ti_2C and V_2C

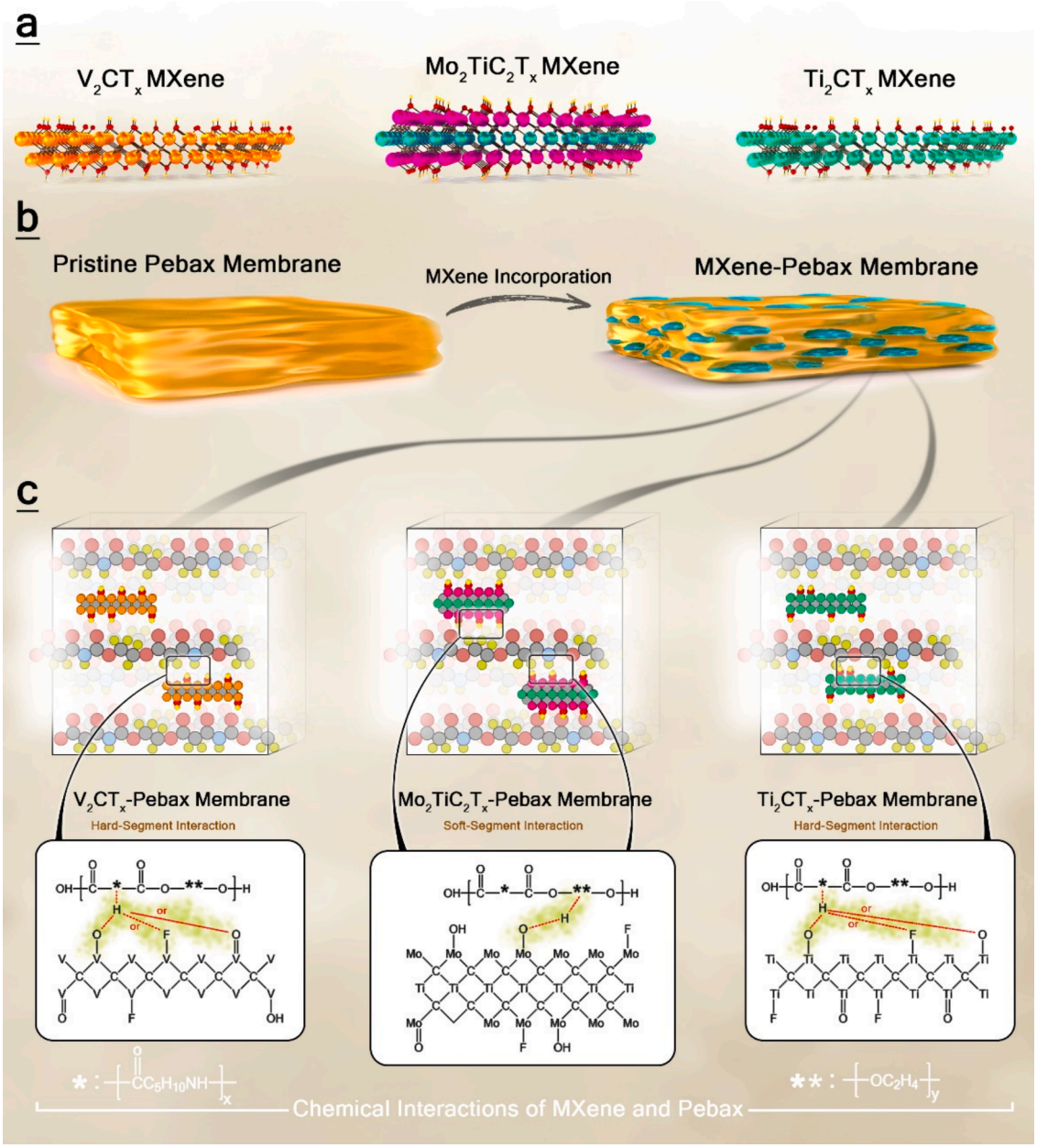

Fig. 4. Schematic representation of the distribution of different MXenes in the hard and soft segments of Pebax based on MXene composition and atomistic structure.

within the crystalline domains of the Pebax matrix (Fig. 3**d**, **Fig. S5b, and Fig. S5c**). Compared to Ti_2C and V_2C (n = 1), the appearance of a boarder peak (shown by * in Fig. 3**d**) with an increased intensity corresponding to the amorphous domain indicates that Mo_2TiC_2 (n = 2) nanosheets gravitate to the soft segment without any change in the crystalline domain (Fig. 3**d**, **Fig. S5a,** and Fig. 4). As the Mo_2TiC_2 content increases in the membrane, the crystalline peak of Pebax broadens (**Fig. S5a**). In addition, an extra domain around $2\theta \sim 6^\circ$ was created by incorporating Mo_2TiC_2 nanosheets in Pebax. The increased amorphousness of the soft bulk can be beneficial to improve the permeability of Mo_2TiC_2-based membranes, but on the other hand, it can be detrimental to the mechanical strength of the membranes. A previous study showed that despite the similar atomistic structure, Ti_3C_2 (n = 2) nanosheets were distributed in the hard segment with a significant decrease in the Pebax crystalline domain.[19] This analysis demonstrates that for M_2C MXenes (Ti_2C and V_2C), the composition has an insignificant effect on the dispersion of nanosheets in Pebax. On the contrary, the effect of this parameter on M_3C_2 MXenes (Mo_2TiC_2 and Ti_3C_2) is significant. Additionally, this measurement further supports the argument that the atomistic structure (number of n) can dramatically affect the dispersion of MXenes in a copolymer with hard and soft segments. In addition to the number of layers and transition metal type, structural defects and functional groups can significantly influence MXene dispersion. While this study primarily focused on the effect of MXene atomic layer and transition metal type, surface chemistry, functionalization, and defect density can also impact dispersion behavior.

More qualitative differences in the dispersion of MXenes are observed by comparing the elastic modulus and elongation at break of all free-standing membranes incorporated by different concentrations of the three types of MXenes. The incorporation of 0.2 wt% Ti_2C and V_2C increased the elastic modulus by 13–15 % compared to pure Pebax (Fig. 3**e**). The increased elastic modulus is an indication of the presence of interfacial interactions and high compatibility between Ti_2C/V_2C and Pebax. A 30 % increase in elastic modulus was observed for the Pebax-Ti_3C_2 membrane where the Ti_3C_2 nanosheets were similarly dispersed

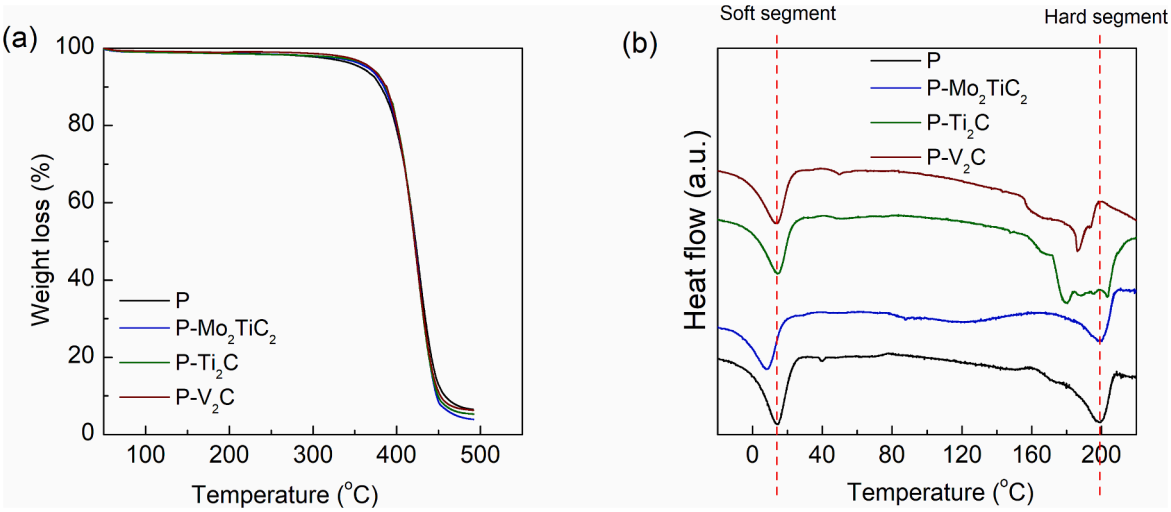

Fig. 5. (a) TGA thermograms, and (b) DSC of MMMs containing 0.2 wt% of each MXene.

mainly in the Pebax hard segments. On the contrary, when 0.2 wt% Mo_2TiC_2 was embedded into the polymer, the elastic modulus of the corresponding MMM decreased by 29 %, which could be related to the increased amorphousness of the soft bulk with the addition of Mo_2TiC_2, which was confirmed by XRD analysis. The disruption of the hard segment created by Ti_2C or V_2C nanosheets reduced the elongation at break of the resulting MMMs (4.5 %), which is lower than the value reported for Pebax-Ti_3C_2 (7.5 %) [19] and can be attributed to the lower disruptive effect of M_2C MXenes compared to M_3C_2 (Mo_2TiC_2 and Ti_3C_2) (Fig. 3**f**). The distribution of Mo_2TiC_2 in the soft segment had almost no effect on elongation at break of Pebax-Mo_2TiC_2 membranes. This finding provides significant insights into how the composition or atomistic structure of MXenes influences the distribution of MXene in copolymers with hard and soft segments.

Thermal stability is almost unchanged due to the low concentration of MXene (Fig. 5**a**). The thermogravimetric analysis (TGA) primarily assesses thermal degradation behavior, where low MXene concentrations could significantly alter the decomposition temperature or weight loss profile due to the dominant contribution of the Pebax matrix. The difference in the dispersion of Mo_2TiC_2 with V_2C can be observed in the differential scanning calorimetry (DSC) thermograms of the pristine Pebax and MMMs (Fig. 5**b**). DSC is highly sensitive to thermal transitions, such as glass transition temperature (Tg) and crystallization behavior, which can be influenced even by small amounts of MXene due to changes in polymer chain mobility and interfacial interactions. Two sharp peaks at 13 °C and 200 °C are attributed to the melting points of the soft and hard segments of Pebax, respectively. The creation of more amorphous regions in the Pebax-Mo_2TiC_2 membrane due to the dispersion of Mo_2TiC_2 in the soft segments resulted in a 7°C lower melting point for the soft segment without changing in the melting point of the hard segment (Fig. 5**b**). On the other hand, no change in the melting point of the soft segments of Pebax-Ti_2C and Pebax-V_2C membranes was observed, but the melting point of the hard segments decreased to 182-187°C, which further confirmed the dispersion of M_2C MXenes (Ti_2C and V_2C) in the Pebax hard segment (Fig. 5**b**).

To indirectly investigate the dispersion of MXene in the polymer, we performed tensile strength tests on free-standing MMMs. The quantitatively similar tensile strength values of all MMMs reflect the uniform distribution of MXene nanosheets in the Pebax matrix (Fig. 3**g**). Similar behavior was observed for Pebax-Ti_3C_2 in a previous study.[19] In addition, the lack of significant change in the tensile strength values of MMMs indicates the high compatibility of the constructive components of the membranes.[19] This analysis shows that the effect of MXene composition or atomistic structure on the dispersion of MXenes in polymer matrices like Pebax is negligible. Most likely, the satisfactory dispersion of MXenes in a polymer can be attributed to the rich surface chemistry of MXene surface, strong interactions of MXene nanosheets with polymer chains, and good dispersion of nanosheets in dope solutions used to fabricate MXene-based MMMs. Moreover, SEM (Fig. 6**)** and atomic force microscopy (AFM) (Fig. 7) analyses show that there is no increase in roughness of the membranes upon the addition of all three types of MXenes, which indicates the good dispersion of the nanosheets in the polymer matrix. In addition, energy-dispersive X-ray spectroscopy (EDX) mapping (Fig. 6) of the main transition metal confirms the satisfactory dispersion of the nanosheets. Moreover, the cross-sectional SEM images (Fig. 6) indicate uniform thickness (92–96 μm) across all membranes and confirmed their consistency.

Here, we investigated the molecular interactions between various MXenes and Pebax using MD simulation (**Fig. S8-S11 and Table S2**, details are given in SI). Negative predicted interaction energies (**Table S3**) indicate the formation of stable configurations especially for Pebax-Mo_2TiC_2 membranes. The presence of functional groups on the MXenes surface and Pebax backbone leads to the formation of bonds at the filler-polymer interfaces. To confirm the formation of hydrogen bonds, the radial distances between the donor and acceptor groups of three types of MXenes and the Pebax chains were calculated, and the interactions are presented in Fig. 8**a**. The shorter overlap distance of MXene/Pebax using Mo_2TiC_2 nanosheets indicates that the functional groups provide more efficient adhesion between the polymer at the MXene surface, and promote robust interactions. Furthermore, the characteristic separation distances of Pebax and V_2C are smaller than those of Pebax and Ti_2C, confirming the predicted more negative interaction energy for Pebax-V_2C (**Table S3**). Moreover, X-ray photoelectron spectroscopy (XPS) spectra of Pebax and the MMMs confirm hydrogen bonding between MXenes and Pebax chains (Fig. 9). The observed shifts in the binding energies of C, O, and N indicate increased electron density around C and N atoms and decreased density around O atoms, suggesting hydrogen bond formation between Pebax's O and N atoms and the –OH, –F, and –O- functional groups on MXenes (Supporting Information, **Table S1**). In addition, the distribution of different MXenes in Pebax was identified using MD simulations. As confirmed by XRD analysis and mechanical strength tests, the Mo_2TiC_2 nanosheets are more distributed in the soft segments of the Pebax than in the hard segments (**Fig. S12**). However, similar to $Ti_3C_2T_x$ reported in a previous study[19], V_2C and Ti_2C interact more with Pebax hard segments (**Fig. S13 and S14**). The results demonstrate proper compatibility and good adhesion between Pebax and MXenes, which leads to the homogeneous dispersion of MXene nanosheets and thus the formation of

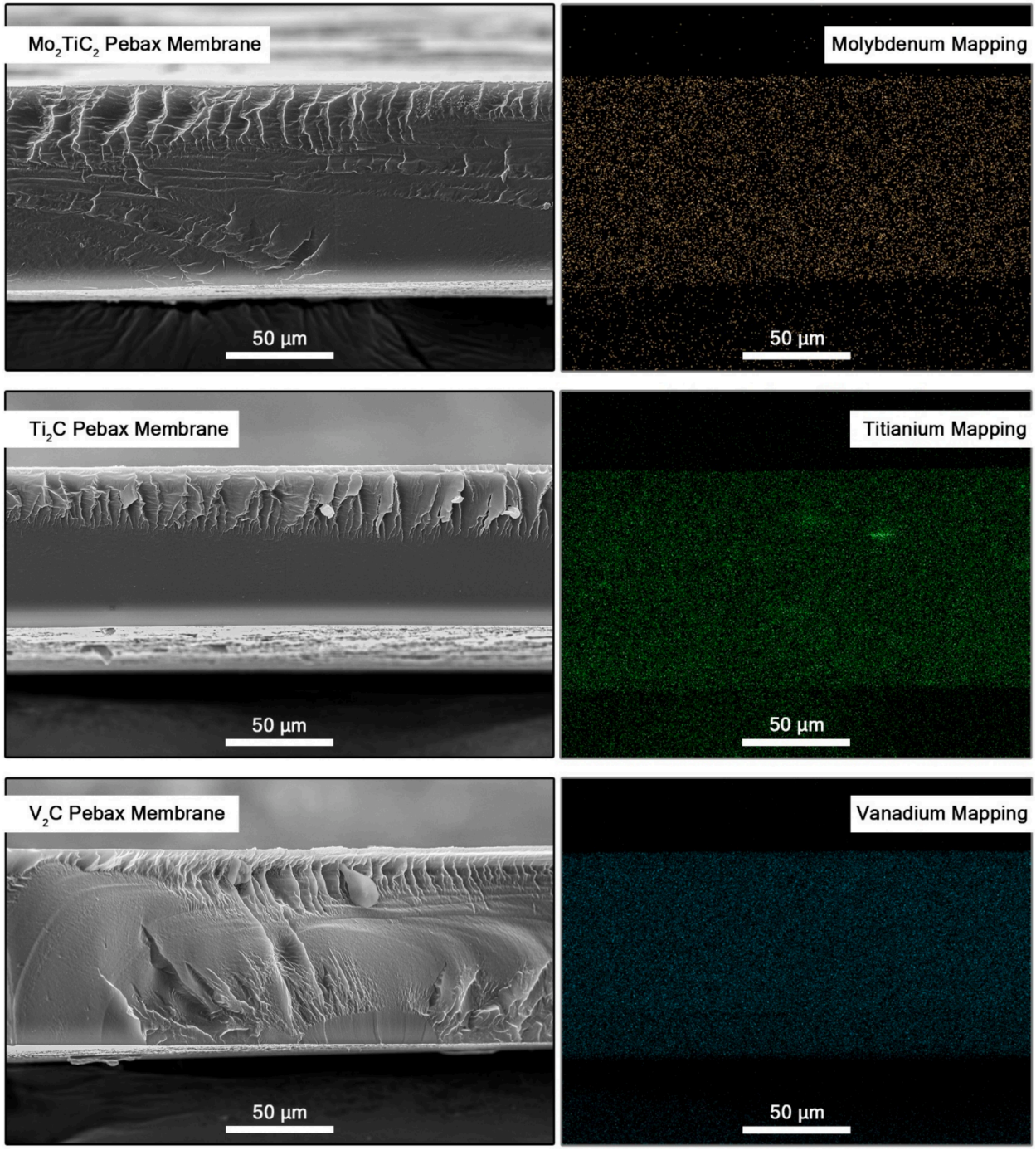

Fig. 6. SEM image (left) and EDX of main transition mapping (right) of (a) Pebax-Mo_2TiC_2, (b) Pebax-Ti_2C, and (c) Pebax-V_2C membranes.

defect-free membranes.

Stimulated by the dispersion dependency of MXenes on the composition and atomistic structure, we performed gas permeation experiments at 25 °C and 4 bar with CO_2 and N_2 pure feed gas. The addition of MXenes with different compositions and atomistic structures to Pebax led to a simultaneous increase in CO_2 permeability and CO_2/N_2 selectivity (Fig. 10**a**). Similar behavior was observed in previous reports, [19,22,23] indicating the high compatibility and strong interactions of the MXenes-Pebax interface, as evidenced by our modeling and MD simulations. The loading was optimized by incorporating 0–0.2 wt% of each MXene in the Pebax matrix. The highest CO_2 permeabilities of 137, 110, and 114 barrer were obtained for each series of MMMs upon loading of 0.075 wt% Mo_2TiC_2, 0.05 wt% Ti_2C, and 0.1 wt% V_2C in the Pebax matrix, respectively (**Tables S4-S7**). The values are equivalent to 71 %, 36 %, and 42 % increase in CO_2 permeability of Pebax-Mo_2TiC_2, Pebax-Ti_2C, and Pebax-V_2C membranes compared to the pristine Pebax membrane, respectively. Based on our experimental findings, the optimal MXene loading varies depending on the specific MXene composition. 0.05 wt% for Ti_2C, 0.075 wt% for Mo_2TiC_2, and 0.1 wt% for V_2C resulted in the best gas separation performance (Fig. 10**d, and Fig. S16-S18**). These concentrations provided a decent balance between enhanced molecular sieving properties and maintaining good dispersion within the Pebax matrix. Beyond these concentrations, excessive MXene loading led to nanosheet agglomeration, reducing the effective transport pathways and negatively impacting permeability and selectivity. This behavior aligns with previous reports on 2D nanomaterial-polymer

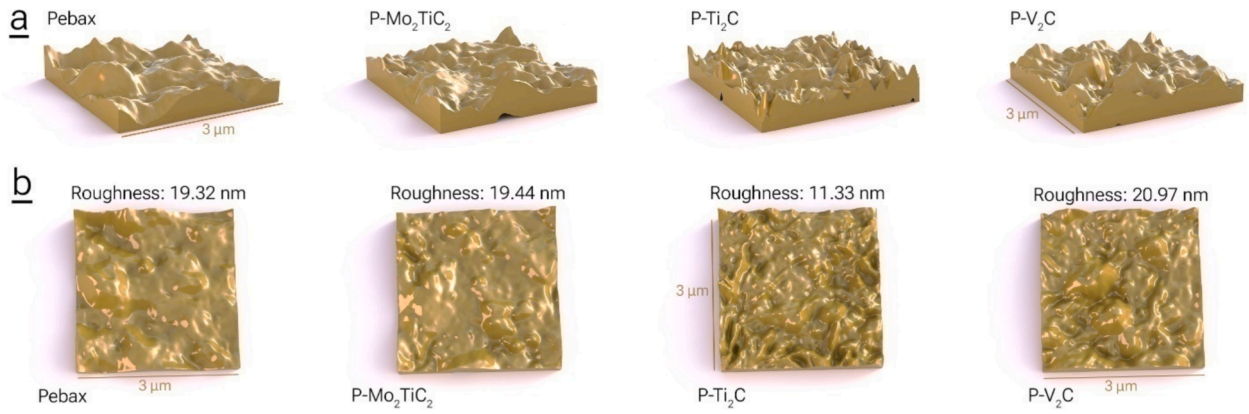

Fig. 7. (a) The cross angle, and (b) top angle 3-dimensional AFM images of membranes.

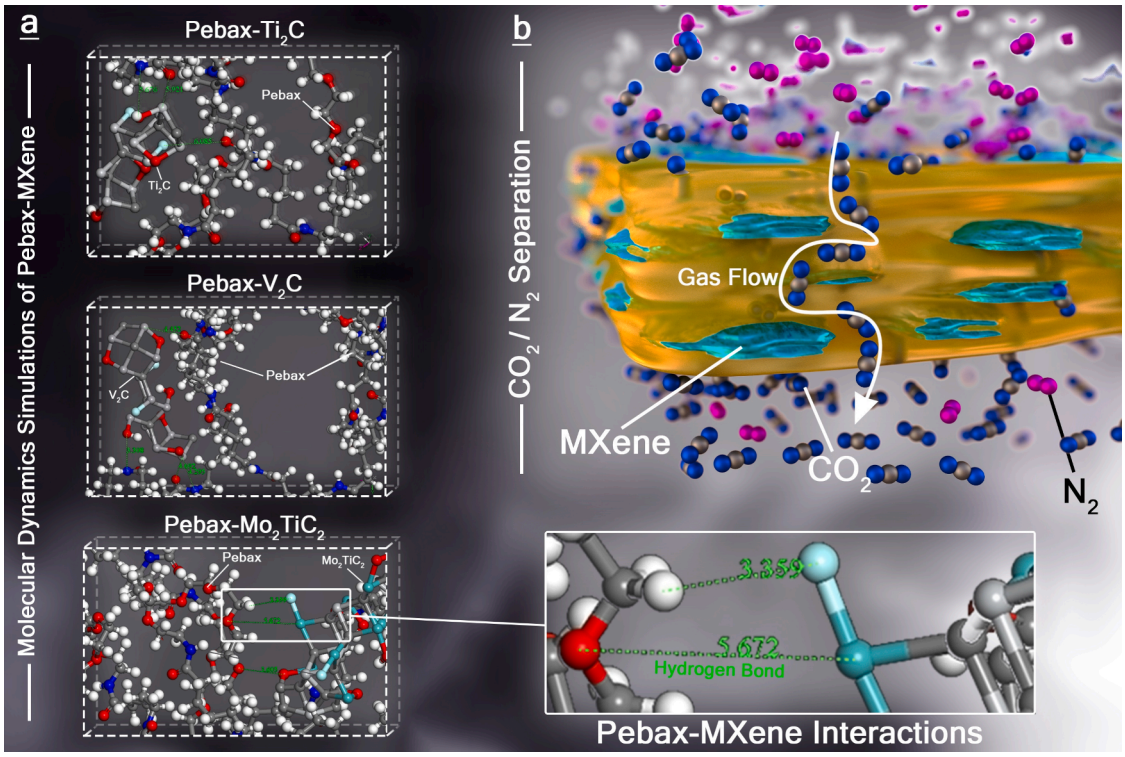

Fig. 8. A) interfacial interactions between Pebax and Mo_2TiC_2, Pebax and Ti_2C, Pebax and V_2C, and (b) schematic representation of CO_2 and N_2 molecules transport through Pebax-MXenes membranes (C, grey; O, red; N, blue; Mo, Cyan; Ti, light gray; V, dark gray; H, white).

composites, where an optimal loading threshold exists before performance declines due to agglomeration effects. A similar effect was previously observed in our study at 0.1 wt% for Ti_3C_2.[19] To elucidate the governing gas transport mechanisms, we deconvoluted gas permeabilities into solubility coefficients (solubility, S) and diffusion coefficients (diffusivity, D) based on the so-called solution-diffusion model.[36,37] The adsorption isotherms of the membranes were used to obtain the solubility coefficients, and then the diffusivity coefficients were calculated based on the relationship between P, D, and S. The addition of various MXenes with different loadings to Pebax increased the solubility coefficients of CO_2 in MMMs due to the high affinity of CO_2 to MXenes resulting from the high quadrupole moment of CO_2 molecules (Fig. 10**b**, Table S4-S7). First-principles density functional theory showed a greater affinity for CO_2 molecules toward MXenes compared to N_2.[38] This factor can increase the CO_2 solubility coefficient of all MXene-based MMMs and thus the CO_2 permeability (Fig. 8**b**). However, N_2 solubility coefficients remained constant with the addition of different MXenes with different loadings (Fig. 10**b**). On the other hand, the N_2 diffusion coefficients decreased due to obstruction effects provided by the MXene nanosheets. On the contrary, all MMMs incorporated by various MXenes demonstrated a higher CO_2 diffusion coefficient than the pristine Pebax, leading to improved CO_2 permeability (Fig. 10**c**). The enhanced diffusion of CO_2 can be ascribed to the molecular sieving of MXene nanosheets as well as the creation of more free volume in MMMs confirmed by MD simulations (Fig. 8, and Table S2). The dispersion of V_2C and Ti_2C in the Pebax hard segment, which was confirmed by XRD analysis and MD simulations, increases the microphase separations and forms more pathways for CO_2 transport. Due to the amorphous domains and the additional domain with the addition of Mo_2TiC_2 nanosheets discussed in the XRD analysis, Pebax-Mo_2TiC_2 indicated showed the highest fractional free volume (FFV) calculated by MD simulation among other MMMs and the pristine Pebax (Table S2). Field visions of FFV for the pristine polymer and MMMs are presented in Fig. S15. The order of FFV is Pebax-Mo_2TiC_2 > Pebax–V_2C > Pebax–Ti_2C > Pebax,

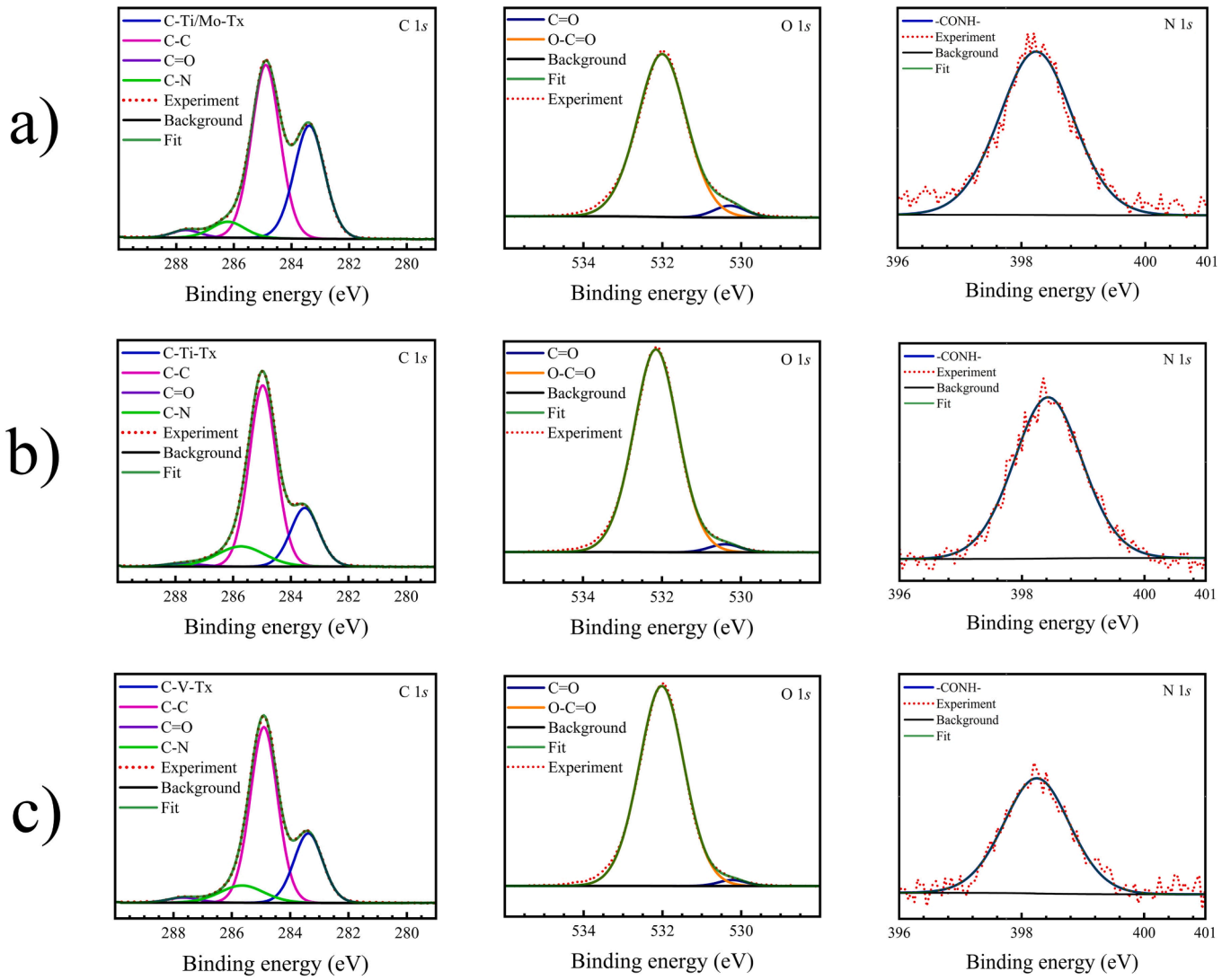

Fig. 9. C 1 s, O 1 s, and N 1 s XPS spectra for (a) Pebax-Mo_2TiC_2 membrane, (b) Pebax-Ti_2C membrane, and (c) Pebax-V_2C membrane.

which follows the diffusion coefficients of the respective membranes. In addition to the channels formed between the MXene layers, the disruption of the polymer chains in the hard segments in the case of V_2C and Ti_2C and the creation of more amorphous regions in the Pebax-Mo_2TiC_2 membranes resulted in a higher FFV of MMMs compared to pristine Pebax.

To evaluate the compatibility of MXenes with Pebax, the prominent Maxwell [39], Chiew-Glandt [40], and Felske [41] models were used to predict the CO_2 and N_2 permeability data of MMMs incorporated by the three MXenes (details are given in the SI). The lack of deviation of the predicted values from the experimental gas permeability data indicates the excellent compatibility of all MXenes with Pebax chains (Fig. 10**d**, Fig. S16-S18). In addition to predicting the gas permeabilities permeability through MD simulations, the solubility coefficients of gas molecules in the pristine membrane and MMMs were obtained from the slope of the adsorption isotherms[42], and the diffusion coefficients of gas molecules were determined using Einstein's equation[43] from the mean squared displacement (MSD) curve (details are given in the SI). In addition to the modeling data, very close gas performance data obtained from MD simulations confirm the excellent compatibility of all three MXenes with Pebax chains (Table S4).

Interestingly, the highest CO_2/N_2 selectivities of 102, 79, and 83 were obtained for the membranes showing the highest CO_2 permeability, over 137 %, 84 %, and 93 % higher than pristine Pebax. The greater solubility of CO_2 molecules in MMMs along with no change in the solubility of N_2 molecules (Fig. 10**b**) led to a higher solubility selectivity of these membranes compared to the pristine membrane. Furthermore, the diffusivity selectivity of all MMMs was extremely improved due to the simultaneous decrease in N_2 diffusivity and increased CO_2 diffusivity (Fig. 10**c**). The presence of MXene nanosheets can restrict the transport of N_2 molecules by increasing the tortuosity of the molecule pathways and enhance the CO_2 transport through the molecular sieving mechanism, thus leading to a significant increase in CO_2/N_2 diffusivity selectivities and finally CO_2/N_2 selectivities (Fig. 8**b**). The significant increase in selectivities indicates that all three MXenes have favorable interactions with the copolymer matrix, leading to the fabrication of defect-free MMMs. The CO_2/N_2 separation performance of Pebax-Ti_2C-0.05 wt% and Pebax-V_2C-0.1 wt% places them in the vicinity of the (above) and very close to the 2008 Robeson upper bound (Fig. 10**a**). Despite the differences in composition and synthesis method, similar dispersion behavior, mechanical strength, and transport properties were observed for Pebax-Ti_2C and Pebax-V_2C MMMs. These results demonstrate no significant effect of the composition of M_2C (n = 1) MXenes on the physical and transport properties of their corresponding MMMs. The excellent CO_2/N_2 selectivity of 102 and CO_2 permeability of 137 barrer for Pebax-Mo_2TiC_2-0.075 wt% placed this membrane well above the 2008 Robeson upper bound, even higher than the performance of previously reported prominent Pebax-Ti_3C_2

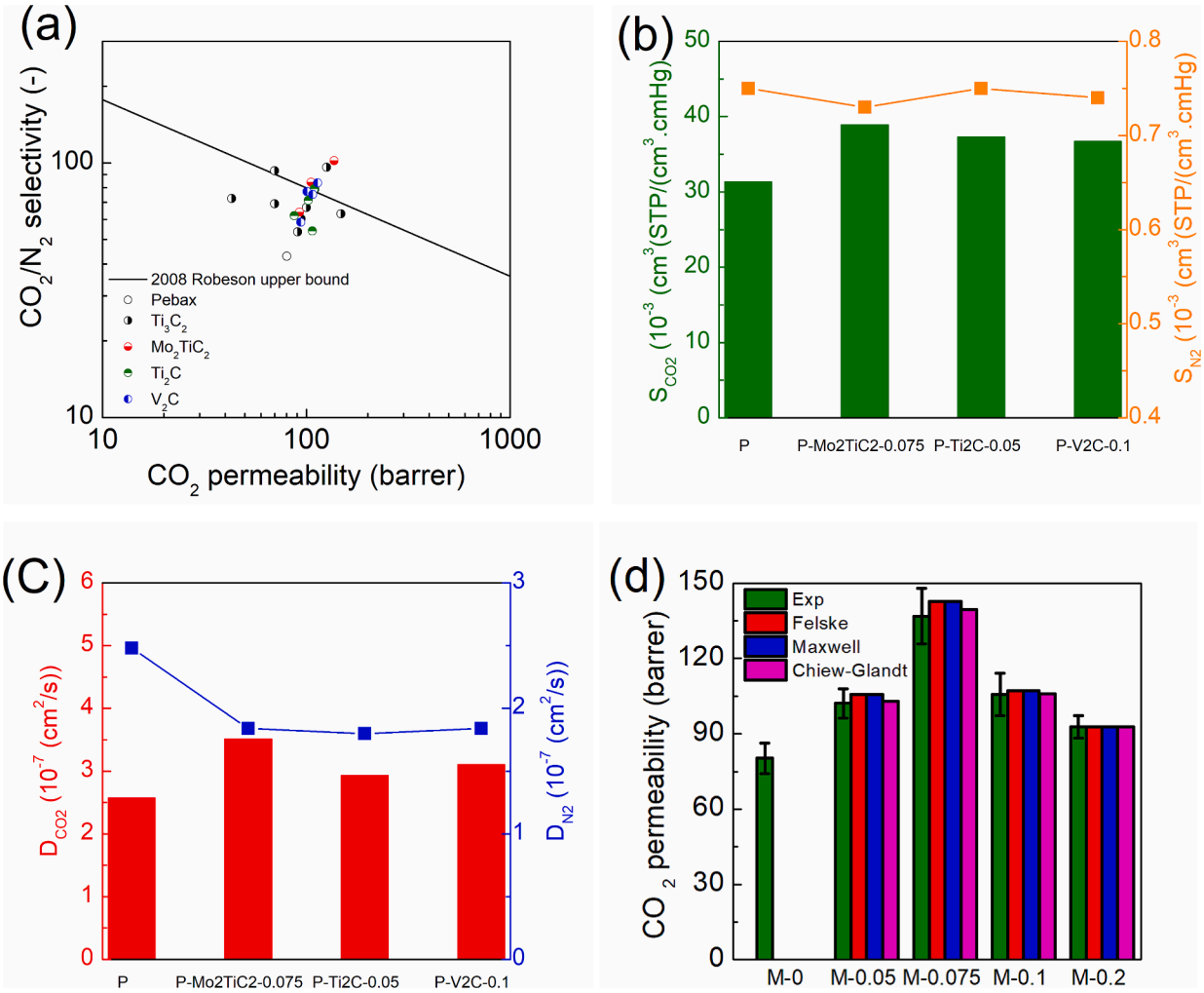

Fig. 10. (a) CO_2/N_2 transport properties of the Pebax-Mo_2TiC_2, Pebax-Ti_2C, and Pebax-V_2C MMMs relative to the pristine Pebax, Pebax-Ti_3C_2 (previous studies) [19,22,23,44,45], and the 2008 Robeson upper under, (b) CO_2 and N_2 solubility coefficients for the free-standing MMMs (P is Pebax) with the highest CO_2 permeability and CO_2/N_2 selectivity and the pristine polymer, (c) CO_2 and N_2 diffusivity coefficients for the free-standing MMMs with the highest CO_2 permeability and CO_2/N_2 selectivity and the pristine polymer, and (d) CO_2 permeabilities of Pebax-Mo_2TiC_2 membranes calculated by prominent Maxwell, Felske, and Chiew-Glandt models compared to those of the experimental data.

membranes (Fig. 10**a**). Compared with M_2C (n = 1) MXenes (Ti_2C and V_2C), the effect of M_3C_2 (n = 2) MXenes (Mo_2TiC_2 and Ti_3C_2) on Pebax membrane performance was more significant. In addition, changing 2 layers of Ti with Mo had a positive effect on the performance of the membrane. To the best of our knowledge, our results provide the first experimental attempt to correlate the composition and atomistic structure of MXenes with their physical and transport properties in MMMs. Compared to the separation performance of different Pebax-based MMMs reported in the literature (**Table S9**), the Pebax–Mo_2TiC_2 membrane with 0.075 wt% filler shows outstanding efficiency for CO_2 capture, achieving a CO_2 permeance of 137 Barrer and a CO_2/N_2 selectivity of approximately 102. MXenes have polar functional groups (e.g., –OH, –F) that increase CO_2 sorption selectivity and improve gas separation efficiency by forming hydrogen bonds with CO_2 molecules. [46] The nature and density of the surface terminations significantly affects CO_2 affinity, and targeted surface modifications can further enhance performance. [47,48] The robust metallic bonds (M−T) in MXenes contribute to high electrical conductivity and mechanical stability. [49] Their metastable nature allows for the tuning of interlayer spacing and surface chemistry, optimizing gas separation properties. [50,51] The interlayer distance plays an important role in molecular sieving efficiency. [52] The composition and structure of MXenes influence the formation of nanochannel and the molecular sieving effect, which is essential for achieving excellent selectivity and permeability in MMMs. [53,54] MXenes offer tunable surface chemistry and high aspect ratios that facilitate dispersion and interaction with the polymer matrix. [55] Nonetheless, they are more susceptible to oxidation and require careful handling to prevent degradation. [56,57] Carbon nanotubes (CNTs) and graphene have mechanical strength, but MXenes exhibit greater hydrophilicity and CO_2 affinity due to their surface functionalities. [45,58] Graphene oxide (GO) can offer comparable functions; nevertheless, it does not have the conductivity of MXenes. [59,60] MXenes have advantages including adjustable surface chemistry, elevated aspect ratio, and mechanical strength, which improve CO_2 interaction and promote superior dispersion and interfacial contact within the polymer matrix. [53,61,62] However, they possess drawbacks such as agglomeration, oxidation, and high costs compared to conventional fillers like silica or carbon black. [63,64].

Feed pressure plays an important role in influencing gas permeability in rubbery polymer matrices.[65] As depicted in Fig. 11**a**, the CO_2 permeability of both pure Pebax and the MMMs shows a significant increase with increasing feed pressure. This can be attributed to the strong interaction between the ether groups in the membranes and the CO_2 molecules due to the quadrupole-dipole moment force. Additionally, high pressure increases the driving force and solubility of CO_2 in the membrane[66], which has a greater impact than membrane

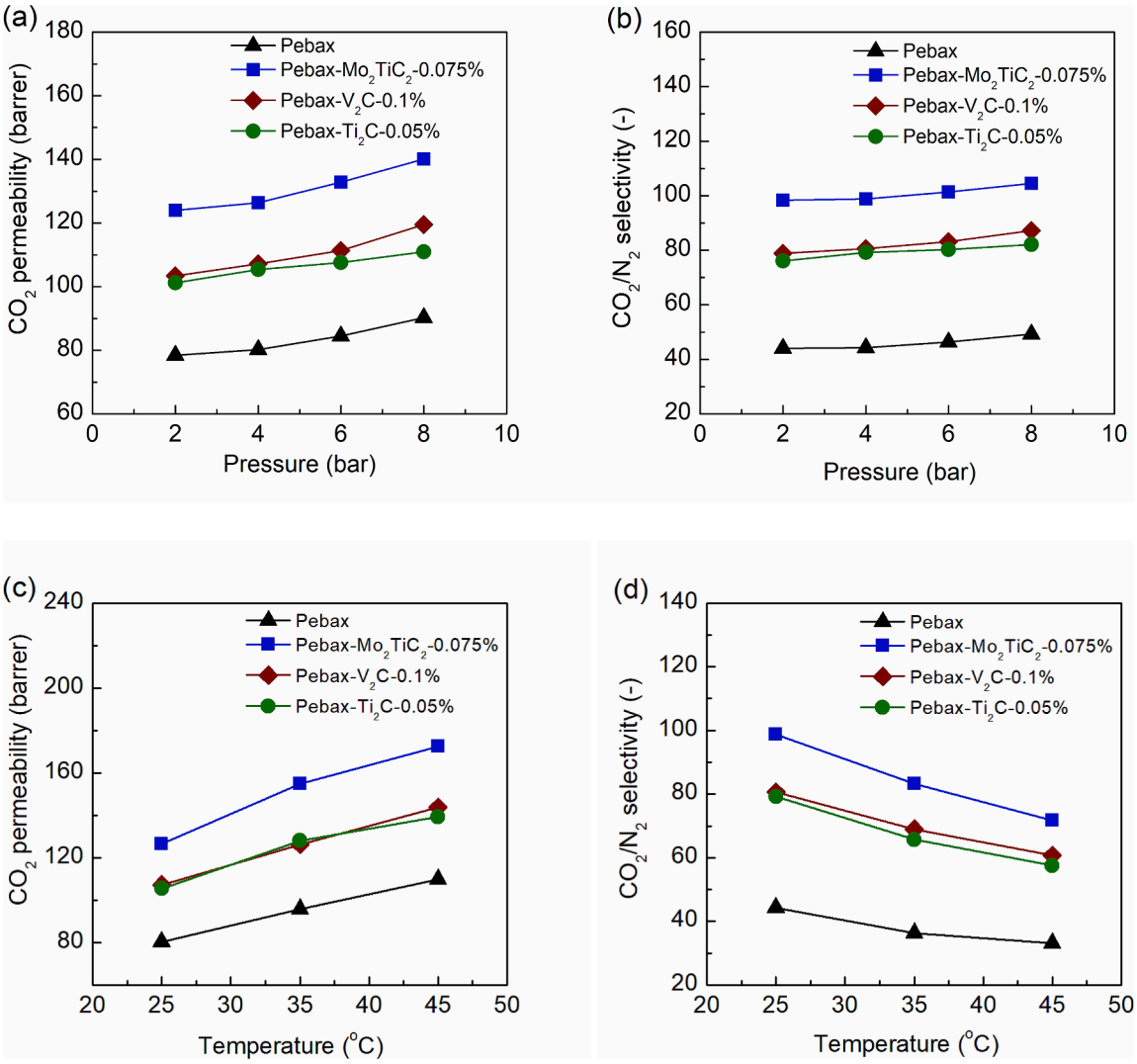

Fig. 11. (a) CO_2 permeability of membranes at various pressures and 25 °C, (b) CO_2/N_2 selectivity of membranes at various pressures and 25 °C, (c) CO_2 permeability of membranes at different temperatures and 4 bar, and (d) CO_2/N_2 selectivity of membranes at different temperatures and 4 bar.

densification. While increasing pressure may decrease the free volume fraction and reduce gas diffusivity, the overall effect is to increase CO_2/N_2 selectivity with increasing pressure (Fig. 11**b**).

Fig. 11**c** shows that both CO_2 and N_2 permeabilities increase with increasing feed temperature. With the increase in temperature, the thermodynamic energy, mobility and diffusion energy of gas molecules also increase, which leads to an increase in permeability. Furthermore, high temperatures improve the flexibility of polymer chains and increase the free volume fraction and facilitate the transport of gas molecules.[67] Gas permeation through membranes is considered a temperature-activated process and follows the Arrhenius equation. [68] The permeation activation energy (Ep) for CO_2 (11.00–12.35 kJ/mol) and N_2 (22.80–23.95 kJ/mol) (**Table S8**) shows that N_2 permeability is more sensitive to temperature changes than CO_2. This sensitivity indicates that N_2 permeation is more temperature-dependent, resulting in a decrease in CO_2/N_2 selectivity at higher temperatures, as shown in Fig. 11**d**.

The mixed gas separation performance of pure Pebax and MMMs with optimized filler concentrations (Pebax-Mo_2TiC_2-0.075 %, Pebax-Ti_2C-0.05 %, and Pebax-V_2C-0.1 %) was evaluated using a CO_2/N_2 (30/70 vol/vol%) mixed gas feed at 25 °C and 4 bar, as shown in Fig. 12**a,b**. CO_2 permeability and CO_2/N_2 selectivity in the mixed gas experiments were lower compared to the pure gas measurement results. This reduction can be attributed to the competitive interactions between the two gases and non-ideal effects present in mixed gas experiments, as noted in previous studies [37,69]. Such behavior is a common trend for rubbery polymers and many glassy polymers, as reported in the literature [70]. Furthermore, the MMMs retain their high separation performance even after 9 months of storage, as shown in Fig. 12**c,d**. This long-term stability highlights the membrane's exceptional chemical and structural durability with no physical aging, which is further supported by the effective shielding of the MXene surface by Pebax chains, preventing the oxidation of MXene nanoflakes, as observed in previous studies. [19,71].

Sensitivity analysis was performed presenting first-order and the total-effect Sobol indices corresponding to each parameter considered in the analysis (**Table S10**, details are given in Supporting Information). The findings are shown in Fig. 13 through a bar plot, which provides a clear visual representation of the impact of input parameters on the model output. Sobol sensitivity analysis elucidates fundamental insights into the influence of operational and structural parameters on gas permeation in MXene-Pebax MMMs. Feed flow rate is the primary factor showing first-order indices of 0.999587, indicating changes in flow rate directly affecting gas residence time and convective transport, [72,73] accounting for approximately 99.96 % of the output variance. Likewise, membrane area shows a significant first-order effect (0.98346), as

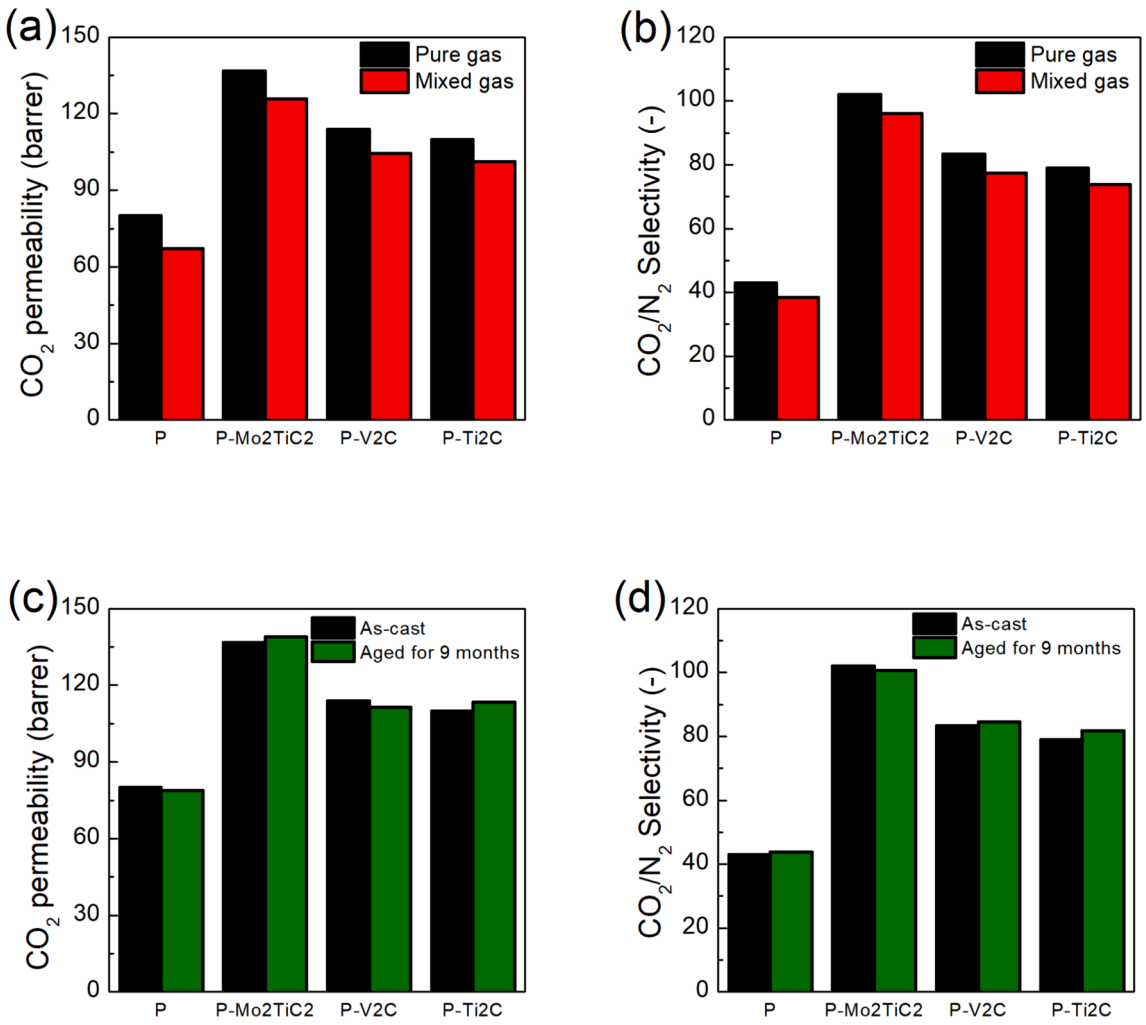

Fig. 12. Comparison of (a) CO_2 permeability for pure and mixed gases of Pebax and MMMs with optimized filler contents, (b) CO_2/N_2 selectivity for pure and mixed gases of Pebax and MMMs with optimized filler contents, (c) CO_2 permeability of as-cast and 9-month aged Pebax and MMMs with optimized filler contents, and (d) CO_2/N_2 selectivity of as-cast and 9-month aged Pebax and MMMs with optimized filler contents.

increasing surface area inherently increases the permeate flux. Feed pressure significantly affects the results (first-order indices 0.87775) and is significant due to its considerable interaction effects, as indicated by total effect indices exceeding 1 (1.2778). This indicates that pressure interacts with factors such as membrane thickness or temperature, potentially enhancing phenomena like pressure-induced plasticization or compaction, which change membrane morphology and gas diffusion pathways. [74–76] In addition to these dominant factors, membrane thickness and temperature exhibit complex behavior. Membrane thickness shows a moderate individual effect (first-order indices 0.29555) but significant interactions (total-effect indices 0.70445), indicating that decreasing membrane thickness increases permeance while potentially weakening mechanical stability under pressure or stress. [77,78] Temperature, although significantly influential by itself (first-order indices 0.75194 due to its effect on polymer chain mobility and gas diffusivity [80]), shows reduced combined effects (total-effect indices 0.24806), which is likely attributed to opposing interactions such as thermal expansion opposing pressure-induced compaction. [79] Anomalies in the results, such as the total-effect indices being lower than the first-order indices for flow rate, area, and temperature, contradict the conventional Sobol hierarchy. [80,81]. This may arise from computational estimation inaccuracies, nonlinear model dynamics, or restricted parameter ranges (e.g., physical constraints on flow rate), requiring additional validation. [82].

4. Conclusions

In conclusion, we fabricated a series of MMMs for CO_2/N_2 separation based on Mo_2TiC_2, Ti_2C and V_2C MXenes and Pebax-1657 with improved transport properties. From a novel point of view that has not been explored in any work so far, we reported the first systematic investigation of the effect of MXene composition and atomistic structure on the corresponding membranes. The results of this work led to the revelation of two very important and brilliant criteria for the use of MXenes in membrane gas separation application. The first very important indicator is that the atomistic structure (number of n) can dramatically affect the dispersion of MXenes in a copolymer with hard and soft segments. This means that compared to M_2C (n = 1) MXenes, the use of M_3C_2 (n = 2) MXenes (Mo_2TiC_2 and Ti_3C_2) has more effects on improving membrane separation properties. A second significant indicator is that for M_3C_2 MXenes (Mo_2TiC_2 and Ti_3C_2), composition strongly affects the dispersion of nanosheets in the copolymer, while the effect of this parameter is negligible for M_2C MXenes (Ti_2C and V_2C). This was well revealed by comparing Pebax-Mo_2TiC_2 and the prominent Pebax-Ti_3C_2 composites, that while Mo_2TiC_2 was dispersed in the soft segments of the polymer, Ti_3C_2 with the same atomistic structure and different composition was mainly dispersed in the hard segments of the polymer. On the other hand, the MXene composition did not affect the dispersion of Ti_2C and V_2C MXenes. The 2D structure along with hydrogen bonds at the MXenes-Pebax interfaces contribute to the high

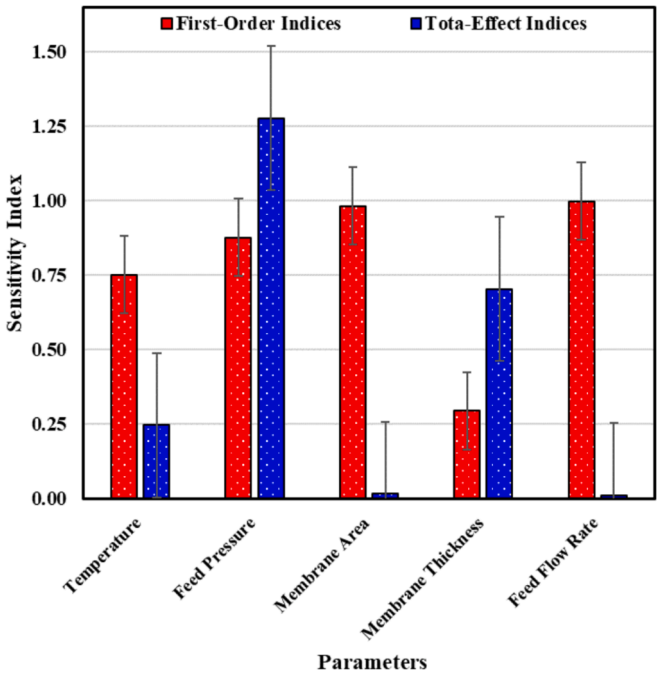

Fig. 13. The first-order and total-effect Sobol indices corresponding to each parameter analyzed in the sensitivity study.

interfacial compatibility in all MMMs, which was confirmed by MD simulations and modeling. Regardless of MXene composition or atomistic structure, MXene nanosheets are well dispersed in the Pebax matrix verified by SEM and AFM. Significant improvements in CO_2 permeability and CO_2/N_2 selectivity and versatile performance were observed for MMMs, placing them above the 2008 Robeson upper bound. Finally, we demonstrated that MXenes have the potential to enhance the gas separation performance of polymeric matrices and that their physical and transport properties can be tuned via MXene composition and atomistic structure.

Declaration of competing interest

The authors declare that they have no known competing financial interests or personal relationships that could have appeared to influence the work reported in this paper.

Appendix A. Supplementary data

Supplementary data to this article can be found online at https://doi.org/10.1016/j.seppur.2025.133360.

Data availability

Data will be made available on request.

References

[1] Z. Liu, W. Qiu, W. Quan, W.J. Koros, Advanced carbon molecular sieve membranes derived from molecularly engineered cross-linkable copolyimide for gas separations, Nat. Mater. (2022) 1–8.
[2] S. Yi, B. Ghanem, Y. Liu, I. Pinnau, W.J. Koros, Ultraselective glassy polymer membranes with unprecedented performance for energy-efficient sour gas separation, Sci. Adv. 5 (2019) eaaw5459.
[3] A. Arabi Shamsabadi, M. Rezakazemi, F. Seidi, H. Riazi, T. Aminabhavi, M. Soroush, Next generation polymers of intrinsic microporosity with tunable moieties for ultrahigh permeation and precise molecular CO_2 separation, Prog. Energy Combust. Sci. 84 (2021) 100903.
[4] S. Zhang, L. Shen, H. Deng, Q. Liu, X. You, J. Yuan, Z. Jiang, S. Zhang, Ultrathin membranes for separations: a new era driven by advanced nanotechnology, Adv. Mater. 34 (2022) 2108457.
[5] Y. Wang, H. Jiang, Z. Guo, H. Ma, S. Wang, H. Wang, S. Song, J. Zhang, Y. Yin, H. Wu, Advances in organic microporous membranes for CO_2 separation, Energ. Environ. Sci. 16 (2023) 53–75.
[6] B. Comesaña-Gándara, J. Chen, C.G. Bezzu, M. Carta, I. Rose, M.-C. Ferrari, E. Esposito, A. Fuoco, J.C. Jansen, N.B. McKeown, Redefining the Robeson upper bounds for CO_2/CH_4 and CO_2/N_2 separations using a series of ultrapermeable benzotriptycene-based polymers of intrinsic microporosity, Energ. Environ. Sci. 12 (2019) 2733–2740.
[7] Y. Dai, Z. Niu, Y. Wang, S. Zhong, P. Mu, J. Li, Recent advances and prospect of emerging microporous membranes for high-performance CO_2 capture, Sep. Purif. Technol. 123992 (2023).
[8] G. Liu, V. Chernikova, Y. Liu, K. Zhang, Y. Belmabkhout, O. Shekhah, C. Zhang, S. Yi, M. Eddaoudi, W.J. Koros, Mixed matrix formulations with MOF molecular sieving for key energy-intensive separations, Nat. Mater. 17 (2018) 283–289.
[9] A. Ebadi Amooghin, S. Mashhadikhan, H. Sanaeepur, A. Moghadassi, T. Matsuura, S. Ramakrishna, Substantial breakthroughs on function-led design of advanced materials used in mixed matrix membranes (MMMs): A new horizon for efficient CO_2 separation, Prog. Mater Sci. 102 (2019) 222–295.
[10] C. Wu, K. Zhang, H. Wang, Y. Fan, S. Zhang, S. He, F. Wang, Y. Tao, X. Zhao, Y.-B. Zhang, Enhancing the gas separation selectivity of mixed-matrix membranes using a dual-interfacial engineering approach, J. Am. Chem. Soc. 142 (2020) 18503–18512.
[11] P.F. Muldoon, S.R. Venna, D.W. Gidley, J.S. Baker, L. Zhu, Z. Tong, F. Xiang, D. P. Hopkinson, S. Yi, A.K. Sekizkardes, Mixed matrix membranes from a microporous polymer blend and nanosized metal–organic frameworks with exceptional CO_2/N_2 separation performance, ACS Mater. Lett. 2 (2020) 821–828.
[12] J.E. Bachman, Z.P. Smith, T. Li, T. Xu, J.R. Long, Enhanced ethylene separation and plasticization resistance in polymer membranes incorporating metal–organic framework nanocrystals, Nat. Mater. 15 (2016) 845–849.
[13] Y. Dai, Z. Niu, W. Luo, Y. Wang, P. Mu, J. Li, A review on the recent advances in composite membranes for CO_2 capture processes, Sep. Purif. Technol. 122752 (2022).
[14] H.E. Karahan, K. Goh, C. Zhang, E. Yang, C. Yıldırım, C.Y. Chuah, M.G. Ahunbay, J. Lee, Ş.B. Tantekin-Ersolmaz, Y. Chen, MXene materials for designing advanced separation membranes, Adv. Mater. 32 (2020) 1906697.
[15] L. Ding, Y. Wei, L. Li, T. Zhang, H. Wang, J. Xue, L.-X. Ding, S. Wang, J. Caro, Y. Gogotsi, MXene molecular sieving membranes for highly efficient gas separation, Nat. Commun. 9 (2018) 155.
[16] J. Shen, G. Liu, Y. Ji, Q. Liu, L. Cheng, K. Guan, M. Zhang, G. Liu, J. Xiong, J. Yang, 2D MXene nanofilms with tunable gas transport channels, Adv. Funct. Mater. 28 (2018) 1801511.
[17] J. Li, X. Li, B. Van der Bruggen, An MXene-based membrane for molecular separation, Environ. Sci. Nano 7 (2020) 1289–1304.
[18] Y. Gogotsi, B. Anasori, The rise of MXenes, in, ACS Publications (2019) 8491–8494.
[19] A. Arabi Shamsabadi, A.P. Isfahani, S.K. Salestan, A. Rahimpour, B. Ghalei, E. Sivaniah, M. Soroush, Pushing Rubbery Polymer Membranes To Be Economic for CO_2 Separation: Embedment with Ti3C2T x MXene Nanosheets, ACS Appl. Mater. Interfaces 12 (2019) 3984–3992.
[20] A. Arabi Shamsabadi, F. Seidi, E. Salehi, M. Nozari, A. Rahimpour, M. Soroush, Efficient CO_2-removal using novel mixed-matrix membranes with modified TiO_2 nanoparticles, J. Mater. Chem. A 5 (2017) 4011–4025.
[21] E. Ghasemi Estahbanati, M. Omidkhah, A. Ebadi Amooghin, Interfacial design of ternary mixed matrix membranes containing Pebax 1657/silver-nanopowder/[BMIM][BF4] for improved CO_2 separation performance, ACS Appl. Mater. Interfaces 9 (2017) 10094–10105.
[22] G. Liu, L. Cheng, G. Chen, F. Liang, G. Liu, W. Jin, Pebax-Based Membrane Filled with Two-Dimensional Mxene Nanosheets for Efficient CO_2 Capture, Chem. Asian J. 15 (2020) 2364–2370.
[23] W. Guan, X. Yang, C. Dong, X. Yan, W. Zheng, Y. Xi, X. Ruan, Y. Dai, G. He, Prestructured MXene fillers with uniform channels to enhance CO_2 selective permeation in mixed matrix membranes, J. Appl. Polym. Sci. 138 (2021) 49895.
[24] W. Luo, Z. Niu, P. Mu, J. Li, Pebax and CMC@ MXene-Based Mixed Matrix Membrane with High Mechanical Strength for the Highly Efficient Capture of CO_2, Macromolecules 55 (2022) 9851–9859.
[25] H. Kim, B. Anasori, Y. Gogotsi, H.N. Alshareef, Thermoelectric properties of two-dimensional molybdenum-based MXenes, Chem. Mater. 29 (2017) 6472–6479.
[26] C. Si, K.-H. Jin, J. Zhou, Z. Sun, F. Liu, Large-gap quantum spin Hall state in MXenes: d-band topological order in a triangular lattice, Nano Lett. 16 (2016) 6584–6591.
[27] S. Huang, V.N. Mochalin, Understanding chemistry of two-dimensional transition metal carbides and carbonitrides (MXenes) with gas analysis, ACS Nano 14 (2020) 10251–10257.
[28] T. Hu, M. Hu, Z. Li, H. Zhang, C. Zhang, J. Wang, X. Wang, Covalency-dependent vibrational dynamics in two-dimensional titanium carbides, Chem. A Eur. J. 119 (2015) 12977–12984.
[29] C. Roy, S.K. De, P. Banerjee, S. Pradhan, S. Bhattacharyya, Investigating suitable medium for the long-duration storage of Ti_2CT_x MXene, J. Alloy. Compd. 938 (2023) 168471.
[30] A. Champagne, L. Shi, T. Ouisse, B. Hackens, J.-C. Charlier, Electronic and vibrational properties of V_2C-based MXenes: From experiments to first-principles modeling, Phys. Rev. B 97 (2018) 115439.
[31] B. Wang, A. Zhou, F. Liu, J. Cao, L. Wang, Q. Hu, Carbon dioxide adsorption of two-dimensional carbide MXenes, J. Adv. Ceram. 7 (2018) 237–245.
[32] Q. Deng, X. Zhao, Q. Zhu, M. Bo, Y. Feng, Reinforced dielectric response in polymer/V_2C MXene composite high-insulation films enabled through dispersing ionic liquid, J. Electroceram. 46 (2021) 124–130.

[33] B. Anasori, M.R. Lukatskaya, Y. Gogotsi, 2D metal carbides and nitrides (MXenes) for energy storage, Nat. Rev. Mater. 2 (2017) 1–17.
[34] P. Bärmann, L. Haneke, J.M. Wrogemann, M. Winter, O. Guillon, T. Placke, J. Gonzalez-Julian, Scalable synthesis of MAX phase precursors toward titanium-based MXenes for lithium-ion batteries, ACS Appl. Mater. Interfaces 13 (2021) 26074–26083.
[35] Y. Shen, H. Wang, X. Zhang, Y. Zhang, MoS_2 nanosheets functionalized composite mixed matrix membrane for enhanced CO_2 capture via surface drop-coating method, ACS Appl. Mater. Interfaces 8 (2016) 23371–23378.
[36] J.G. Wijmans, R.W. Baker, The solution-diffusion model: a review, J. Membr. Sci. 107 (1995) 1–21.
[37] W. Koros, G. Fleming, S. Jordan, T. Kim, H. Hoehn, Polymeric membrane materials for solution-diffusion based permeation separations, Prog. Polym. Sci. 13 (1988) 339–401.
[38] Á. Morales-García, A. Fernández-Fernández, F. Viñes, F. Illas, CO_2 abatement using two-dimensional MXene carbides, J. Mater. Chem. A 6 (2018) 3381–3385.
[39] P.J.A.M. Kerkhof, A modified Maxwell-Stefan model for transport through inert membranes: the binary friction model, Chem. Eng. J. Biochem. Eng. J. 64 (1996) 319–343.
[40] Y.C. Chiew, E.D. Glandt, The effect of structure on the conductivity of a dispersion, J. Colloid Interface Sci. 94 (1983) 90–104.
[41] J.D. Felske, Effective thermal conductivity of composite spheres in a continuous medium with contact resistance, Int. J. Heat Mass Transf. 47 (2004) 3453–3461.
[42] E. Tocci, A. Gugliuzza, L. De Lorenzo, M. Macchione, G. De Luca, E. Drioli, Transport properties of a co-poly(amide-12-b-ethylene oxide) membrane: A comparative study between experimental and molecular modelling results, J. Membr. Sci. 323 (2008) 316–327.
[43] J.C. Zhao, Diffusion Multiple Screening: Phase Diagram Determination and Related Studies, in: K.H.J. Buschow, R.W. Cahn, M.C. Flemings, B. Ilschner, E.J. Kramer, S. Mahajan, P. Veyssière (Eds.), Encyclopedia of Materials: Science and Technology, Elsevier, Oxford, 2005, pp. 1–13.
[44] D. Wang, Y. Xin, Y. Wang, X. Li, H. Wu, W. Zhang, D. Yao, H. Wang, Y. Zheng, Z. He, A general way to transform $Ti_3C_2T_x$ MXene into solvent-free fluids for filler phase applications, Chem. Eng. J. 409 (2021) 128082.
[45] F. Shi, J. Sun, J. Wang, M. Liu, Z. Yan, B. Zhu, Y. Li, X. Cao, MXene versus graphene oxide: Investigation on the effects of 2D nanosheets in mixed matrix membranes for CO_2 separation, J. Membr. Sci. 620 (2021) 118850.
[46] K. Wang, D. Chen, J. Tang, Z. Hong, Z. Zhu, Z. Yuan, Z. Lin, Y. Liu, R. Semiat, X. He, PIM-1-based membranes mediated with CO_2-philic MXene nanosheets for superior CO_2/N_2 separation, Chem. Eng. J. 483 (2024) 149305.
[47] M. Mozafari, S. Khoshhal Salestan, A. Arabi Shamsabadi, K. Jha, M. Tanwar, H. Kim, Z. Fakhraai, M. Soroush, Substantially Improving CO_2 Permeability and CO_2/CH_4 Selectivity of Matrimid Using Functionalized-$Ti_3C_2T_x$, ACS Appl. Mater. Interfaces 17 (2025) 3897–3910.
[48] X. Li, M. Zhan, Y. Liu, W. Tu, H. Li, MXene Synthesis and Carbon Capture Applications: Mini-Review, Chem. Eur. J. 30 (2024) e202400874.
[49] J. Park, M. Kim, H. Kim, J. Lee, I. Lee, H. Park, A. Lee, K. Min, S. Lee, Exploring the large chemical space in search of thermodynamically stable and mechanically robust MXenes via machine learning, PCCP 26 (2024) 10769–10783.
[50] L. Dai, J. Zhao, Q. Li, M. Chen, H. Li, K. Qu, R. Li, Understanding the tunable sodium storage performance in pillared MXenes: a first-principles study, PCCP 24 (2022) 27184–27194.
[51] X. Qiu, L. Dai, H. Li, K. Qu, R. Li, Pillaring Behavior of Organic Molecules on MXene: Insights from Molecular Dynamics Simulations, Langmuir 39 (2023) 14912–14921.
[52] J. Shen, G. Liu, Y. Ji, Q. Liu, L. Cheng, K. Guan, M. Zhang, G. Liu, J. Xiong, J. Yang, W. Jin, 2D MXene Nanofilms with Tunable Gas Transport Channels, Adv. Funct. Mater. 28 (2018) 1801511.
[53] Y. Ibrahim, M.M. Zagho, A. ElAlfy, A. Karim, A.A. Elzatahry, Recent advances in retention and permeation of CO_2 gas using MXene based membranes, npj 2D Mater. Appl. 9 (2025) 12.
[54] J. Li, L. Li, Y. Xu, J. Zhu, F. Liu, J. Shen, Z. Wang, J. Lin, MXene nanosheet stacks with tunable nanochannels for efficient molecular separation, Chem. Eng. J. 427 (2022) 132070.
[55] A.E. Mathew, S. Jose, A.M. Babu, A. Varghese, State of the art MOF-composites and MXene-composites: Synthesis, fabrication and diverse applications, Mater. Today Chem. 36 (2024) 101927.
[56] W. Cao, J. Nie, Y. Cao, C. Gao, M. Wang, W. Wang, X. Lu, X. Ma, P. Zhong, A review of how to improve $Ti_3C_2T_x$ MXene stability, Chem. Eng. J. 496 (2024) 154097.
[57] K.P. Marquez, K.M.D. Sisican, R.P. Ibabao, R.A.J. Malenab, M.A.N. Judicpa, L. Henderson, J. Zhang, K.A.S. Usman, J.M. Razal, Understanding the Chemical Degradation of Ti_3C_2T MXene Dispersions: A Chronological Analysis, Small Sci. 4 (2024) 2400150.
[58] G. Li, S. Lian, J. Wang, G. Xie, N. Zhang, X. Xie, Surface chemistry engineering and the applications of MXenes, J. Materiomics 9 (2023) 1160–1184.
[59] R. Gautam, N. Marriwala, R. Devi, A review: Study of Mxene and graphene together, Meas.: Sens. 25 (2023) 100592.
[60] H. Tan, J. Gou, X. Zhang, L. Ding, H. Wang, Sandwich-structured $Ti_3C_2T_x$-MXene/reduced-graphene-oxide composite membranes for high-performance electromagnetic interference and infrared shielding, J. Membr. Sci. 675 (2023) 121560.
[61] A. Khosla, H.T.A. Sonu, K.S. Awan, R. Gaurav, Z. Walvekar, A. Zhao, M. Kaushik, V. C. Khalid, Emergence of MXene and MXene–Polymer Hybrid Membranes as Future-Environmental Remediation Strategies, Adv. Sci. 9 (2022) 2203527.
[62] M. Yahia, D. Refaat, J. Coronas, C. Tellez, Enhancing CO_2/CH_4 separation performance in PIM-1 based MXene nanosheets mixed matrix membranes, Sep. Purif. Technol. 356 (2025) 129825.
[63] K. Gong, K. Zhou, X. Qian, C. Shi, B. Yu, MXene as emerging nanofillers for high-performance polymer composites: A review, Compos. B Eng. 217 (2021) 108867.
[64] H. Wang, Wei, Y. and Ding, L., MXene -Based Membranes for Gas Separation, in: MXene Membranes for Separations, Wiley, 2022, pp. 89-104.
[65] E. Ahmadpour, A. Arabi Shamsabadi, R.M. Behbahani, M. Aghajani, A. Kargari, Study of CO_2 separation with PVC/Pebax composite membrane, J. Nat. Gas Sci. Eng. 21 (2014) 518–523.
[66] S. Saedi, S.S. Madaeni, A. Arabi Shamsabadi, PDMS coated asymmetric PES membrane for natural gas sweetening: effect of preparation and operating parameters on performance, Can. J. Chem. Eng. 92 (2014) 892–904.
[67] E. Ahmadpour, M.V. Sarfaraz, R.M. Behbahani, A. Arabi Shamsabadi, M. Aghajani, Fabrication of mixed matrix membranes containing TiO_2 nanoparticles in Pebax 1657 as a copolymer on an ultra-porous PVC support, J. Nat. Gas Sci. Eng. 35 (2016) 33–41.
[68] A. Arabi Shamsabadi, A. Kargari, M.B. Babaheidari, S. Laki, Separation of hydrogen from methane by asymmetric PEI membranes, J. Ind. Eng. Chem. 19 (2013) 1680–1688.
[69] L. Shao, T.-S. Chung, In situ fabrication of cross-linked PEO/silica reverse-selective membranes for hydrogen purification, Int. J. Hydrogen Energy 34 (2009) 6492–6504.
[70] J. Schultz, K.-V. Peinemann, Membranes for separation of higher hydrocarbons from methane, J. Membr. Sci. 110 (1996) 37–45.
[71] M. Mozafari, S. Khoshhal Salestan, A. Arabi Shamsabadi, K. Jha, M. Tanwar, H. Kim, Z. Fakhraai, M. Soroush, Substantially Improving CO_2 Permeability and CO_2/CH_4 Selectivity of Matrimid Using Functionalized-$Ti_3C_2T_x$, ACS Appl. Mater. Interfaces (2025).
[72] M. Galizia, W.S. Chi, Z.P. Smith, T.C. Merkel, R.W. Baker, B.D. Freeman, 50th Anniversary Perspective: Polymers and Mixed Matrix Membranes for Gas and Vapor Separation: A Review and Prospective Opportunities, Macromolecules 50 (2017) 7809–7843.
[73] A. Katare, S. Kumar, S. Kundu, S. Sharma, L.M. Kundu, B. Mandal, Mixed Matrix Membranes for Carbon Capture and Sequestration: Challenges and Scope, ACS Omega 8 (2023) 17511–17522.
[74] A.I. Osman, Z. Chen, A.M. Elgarahy, M. Farghali, I.M.A. Mohamed, A.K. Priya, H. B. Hawash, P.-S. Yap, Membrane Technology for Energy Saving: Principles, Techniques, Applications, Challenges, and Prospects, Adv. Energy Sustainability Res. 5 (2024) 2400011.
[75] G. Aguilloso, K. Arpia, M. Khan, Z.A. Sapico, E.C. Lopez, Recent Advances in Membrane Technologies for Biogas Upgrading, Engineering Proceedings, in, 2024.
[76] S. Razavi, A. Jakeman, A. Saltelli, C. Prieur, B. Iooss, E. Borgonovo, E. Plischke, S. Lo Piano, T. Iwanaga, W. Becker, S. Tarantola, J.H.A. Guillaume, J. Jakeman, H. Gupta, N. Melillo, G. Rabitti, V. Chabridon, Q. Duan, X. Sun, S. Smith, R. Sheikholeslami, N. Hosseini, M. Asadzadeh, A. Puy, S. Kucherenko, H.R. Maier, The Future of Sensitivity Analysis: An essential discipline for systems modeling and policy support, Environ. Model. Softw. 137 (2021) 104954.
[77] G.L. Jadav, V.K. Aswal, H. Bhatt, J.C. Chaudhari, P.S. Singh, Influence of film thickness on the structure and properties of PDMS membrane, J. Membr. Sci. 415–416 (2012) 624–634.
[78] H.B. Park, J. Kamcev, L.M. Robeson, M. Elimelech, B.D. Freeman, Maximizing the right stuff: The trade-off between membrane permeability and selectivity, Science, 356 (2017) eaab0530.
[79] G. Guenoun, J.-Y. Faou, G. Régnier, N. Schmitt, S. Roux, Thermal cycling of cold-pressed PTFE compacts: Reversible and irreversible behavior, Polym. Test. 75 (2019) 99–106.
[80] Y. Gan, Q. Duan, W. Gong, C. Tong, Y. Sun, W. Chu, A. Ye, C. Miao, Z. Di, A comprehensive evaluation of various sensitivity analysis methods: A case study with a hydrological model, Environ. Model. Softw. 51 (2014) 269–285.
[81] D. Garcia, I. Arostegui, R. Prellezo, Robust combination of the Morris and Sobol methods in complex multidimensional models, Environ. Model. Softw. 122 (2019) 104517.
[82] H. Chhajer, R. Roy, Rationalised experiment design for parameter estimation with sensitivity clustering, Sci. Rep. 14 (2024) 25864.